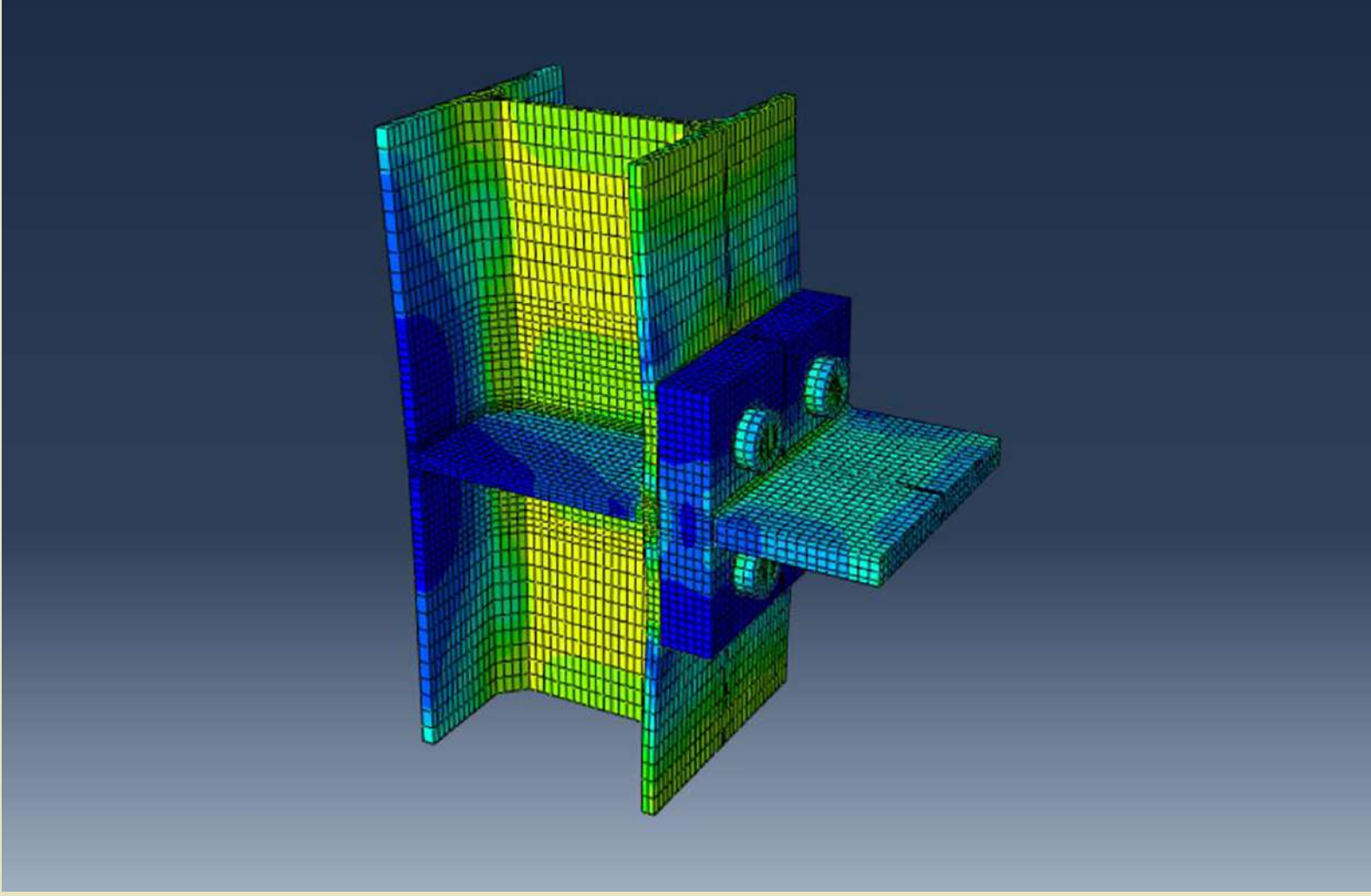

Hafiz Muhammad Ubaid Ur Rehman

FEM ANALYSIS OF THE CYCLIC BEHAVIOUR OF STEEL BEAM-TO-COLUMN JOINTS

Thesis submitted in partial fulfilment of the requirements for SUSCOS_M European Master in Sustainable Constructions under natural hazards and catastrophic events, and supervised by Professor Doctor Luis Alberto Proença Simoes da Silva and Assistant Professor Ricardo Joel Teixeira Costa

February, 2018

· U C ·

Universidade de Coimbra

FEM ANALYSIS OF THE CYCLIC BEHAVIOUR OF STEEL BEAM-TO-COLUMN JOINTS

Author: Hafiz Muhammad Ubaid Ur Rehman, Civil, Engr.

Supervisor: Prof. Luis Alberto Proenca Simoes da Silva, PhD

Asst. Prof. Ricardo Joel Teixeira Costa, PhD

University: University of Coimbra, Coimbra, Portugal

University of Coimbra, Coimbra, Portugal

February, 2018

European Erasmus Mundus Master

Sustainable Constructions under natural hazards and catastrophic events

520121-1-2011-1-CZ-ERA MUNDUS-EMMC

FEM ANALYSIS OF THE CYCLIC BEHAVIOUR OF STEEL BEAM-TO-COLUMN JOINTS

Hafiz Muhammad Ubaid Ur Rehman

February, 2018

Members of the Jury

President:

Prof. Aldina Maria da Cruz Santiago, PhD

Department of Civil Engineering - FCTUC
Rua Luís Reis Santos - Pole II of the University
3030 - 788 Coimbra, Portugal

Thesis Supervisor:

Prof. Luis Alberto Proenca Simoes da Silva, PhD

Department of Civil Engineering - FCTUC
Rua Luís Reis Santos - Pole II of the University
3030 - 788 Coimbra, Portugal

Members:

Prof. Carlos Alberto da Silva Rebelo, PhD

Department of Civil Engineering - FCTUC
Rua Luís Reis Santos - Pole II of the University
3030 - 788 Coimbra, Portugal

Prof. Ricardo Joel Teixeira Costa, PhD

Department of Civil Engineering - FCTUC
Rua Luís Reis Santos - Pole II of the University
3030 - 788 Coimbra, Portugal

ACKNOWLEDGMENT

Thanks ALLAH ALMIGHTY for taking care of me at every step of my life.

The success and final outcome of this project required a lot of guidance and assistance for many people and I am extremely privilege to have got this all along the completion of my dissertation. All that I have done is only due to such supervision and assistance and I would not forget to thank them.

I respect and thank Prof. Luis Alberto Proenca Simoes da Silva, for providing me an opportunity to do the project work within the framework of RFCS project EQUALJOINTS in Institute of Sustainability and Innovation in Structural Engineering (ISISE), University of Coimbra and guiding me, all support and guidance which made me complete the project duly. I am extremely thankful to him for providing such a nice support and direction, although he had busy schedule managing the departmental activities.

I owe my deep gratitude as well to my project co-supervisor Asst. Prof. Ricardo Joel Teixeira Costa, who took keen interest on my project work and guided me all along, till the completion of my project work by providing all the necessary information for developing a good model.

I would not forget to remember Asst. Prof. Helder David Craveiro of Institute of Sustainability and Innovation in Structural Engineering (ISISE), University of Coimbra for his encouragement and more over for his timely support and guidance till the completion of my project work.

I heartily thank my parents, family members and friends who help me a lot in finalizing this project within the limited time frame.

ABSTRACT

The construction of a structure undergoes several stages, each of which must be thoroughly thought. In structures that may be subject to seismic actions at some point of their use life, these considerations are especially significant. Joints between steel elements in this type of structures should always be designed, fabricated and erected such that brittle failure is avoided and a ductile mode of failure governs the collapse.

Designers must always bear in mind design requirements set by the relevant design standards. In Europe, EN1993 must be observed for the seismic design of structures, with significant reference to EN1993 for the design of steel structures and EN1993-1-8 in particular for the design of steel joints making use of the components method.

Nowadays the experimental test is the preferred method between the scientific community to assess the seismic behavior of steel joints. However, the analysis of the seismic behavior of beam-to-columns joints at component level directly from the analysis of the results of the experimental test is unfeasible. Accordingly, advanced numerical models must be developed and validated with the experimental tests.

In this dissertation advanced FEM based models are developed for the analysis of monotonic and cyclic behavior of the tension region of beam-to-column steel joints in the framework of the project “European pre-qualified steel joints (EQUALJOINTS)”, focusing in the behavior of the column flange in bending.

NOTATION

General

t_f	*Flange or plate thickness*
l_{eff}	*Total effective length of an equivalent T-stub*
F	*Force*
$F_{T,\,I,\,Rd}$	*Design resistance for each T-stub mode*
$M_{pl,\,Rd}$	*Resistance of the formed plastic hinges*
$F_{t,\,Rd}$	*Bolt's tension resistance*
m	*Bolt distance to the weld*
n	*Minimum bolt distance to a free edge*
f_y	*Yield strength*
f_u	*Ultimate strength*
f_{ub}	*Bolt ultimate strength*
A_s	*Tensile area of a bolt*
k_2	*Bolt strength reduction factor*
K	*Stiffness*
E	*Elastic modulus*
E_t	*Tangent modulus*

E_u	*Ultimate modulus*
Q	*Prying force*

Greek letters

γ_{Mi}	*Partial safety factor used for applied design situations*
σ_{true}	*True stress*
$\sigma_{engg.}$	*Engineering stress*
ε_{true}	*True strain*
$\varepsilon_{engg.}$	*Engineering strain*
ε_{pl}	*Plastic strain*

Acronyms

MISES	*Von Mises stresses*
PEEQ	*Equivalent plastic strain*

Table of Contents

List of Figures

List of Tables

1. Introduction

1.1 Background

As in all types of structures, the cyclic behavior of beam-to-column steel joints may have a major influence on the performance of moment resisting frames during an earthquake.

However, the analysis and design of steel buildings according to EN 1993-1 [1] and EN 1993-1 [2] may be based on centerline frame models – where the geometry and the mechanical properties of the beam-to-column steel joints is not explicitly modeled – when the beam-to-column joints are full-strength and rigid thus enforcing the formation of dissipative zones near the ends of the beam members [3].

On the other hand, in case of partial strength and/or semi-rigid beam-to-column steel joints, EN 1993-1 [2] allows beam-to-column joints to be the dissipative zones itself. In this case: (i) the joints must have rotation capacity higher than the rotation demands, (ii) the adjacent members framing into the joints must have a stable behavior at ultimate limit conditions and (iii) the effect of the joint deformation on global behavior must be taken into account in the global analysis of structure through a non-linear static (pushover) analysis or non-linear response-history analysis. In this case, refined models, accounting for the beam-to-column joint cyclic behavior, are required for the analysis and design of the structures [3].

EN 1993-1-8 [2] provides a procedure based in the so-called component method to assess the strength and stiffness of beam-to-column joints. However, it does not provide tools to assess neither the rotation capacity nor the cyclic behavior of these structural elements [3].

This work is in the scope of the research project “European pre-qualified steel joints (EQUALJOINTS) Grant agreement no. RFSR-CT-2013-00021” carried out Institute for Sustainability and Innovation in Structural Engineering (ISISE) in University of Coimbra, Coimbra, Portugal.

1.2. Motivation

In order to achieve a good seismic performance of moment resisting frames (MRFs) with reduced costs, these structures are designed to concentrate the dissipation of the energy induced by earthquakes in specific zones so called dissipative zones. In particular, the design of steel moment resisting frames according to EC8, can be carried out by locating the dissipative zones in beams or joints [4]. The location of dissipative zones can be controlled by capacity design according to a strength hierarchy criterion.

In particular, when full strength joints are adopted, joints are designed to be over strength with respect to the connected members and, therefore, the plastic hinges are located at beam ends by means of cyclic inelastic bending, so that dynamic inelastic analyses require the modelling of the cyclic response of the beams where plastic hinges develop. This approach can lead, in some structural situations such as the case of structures with few storeys and/ or with long spans where the design of beams is mainly governed by vertical loads rather than the lateral ones, to column sections significantly greater than those strictly necessary to withstand the member loads [5,6].

On the other hand, partial strength joints can be employed in order to concentrate the plastic zones in the connections. Aforementioned approach is allowed by EC3 [2] which clearly states that the plastic hinges can be developed at the end of the beam or in the joint. In these cases, the response of the joints in term of stiffness, resistance and ductility is a key aspect for design purposes. An analytical procedure to predict the response of joints based on knowledge of mechanical and geometrical properties of individual element of the joint (the components), subjected to static loading condition are available and is known as the "component method". In order to extend the component approach to the prediction of the seismic response of partial strength joints, the modelling of the cyclic response of the joint components is necessary.

In case of bolted connections, the main joint components responsible for the joint ductility, such as the column flange in bending, the end-plate in bending and the angles in tension may be modeled by means of a simplified model known as "T-Stub" [2].

1.3. Main goals and scope

The main goal of this dissertation is the development of advanced Finite Element Models to assess the cyclic behaviour of column flanges in bending of beam-to-column end plate bolted connections. Having into account the complex behaviour of full beam-to-column joints, partial models were used to allow to assess accurately the internal forces and the deformation of the column flange in bending. The models and the load history was define based in the testes and in the findings of EQUALJOINTS project. More in particular, the goal of this dissertation is to assess the influence of the collapse mode of the column flange in bending on its cyclic behaviour. The T-stub model was used as starting point to define the parametric analysis.

2. State of Art

2.1. Behaviour of Joints Under Seismic Load

In MRFs, the seismic resistance of structure should be provided based in a strength hierarchy among members and joints. According to the capacity design concept, such a structure will be able to dissipate part of the energy induced by the ground motion through plastic deformations in the dissipative zones of ductile members, e.g. through bending deformation in beams of Moment Resisting Frames (MRF) – formation of plastic hinges in columns is prevented to avoid the premature collapse of the structure [2] and to allow the mobilization of a large number of dissipative zones by the collapse mechanism. Accordingly, the region where dissipative zones will appear in beams or joints is set by means of an appropriate choice of the ratio between the flexural resistance of the beams and the bending resistance of the joint.

If the dissipative regions are in the beams ends, joints have to be full strength and take into account the possible over strength effects, which leads to expensive joints solutions.

On the other hand, the use of partial strength joint is permitted but the number of requirements to be respected for this joint typology is such that it is currently essential to accomplish experimental tests to check when these requirements are satisfied. The component method is a solution to overcome the “full strength” limitation. This method considers any joint as a set of individual basic component [2] and computes the behaviour of the joint from the behaviour of these basic components.

The probability of forecasting the behaviour of beam to column joints under cyclic loading conditions allows the design of structures able to dissipate the earthquake input energy by means of a stable hysteretic behaviour of beam end and/or of their joints to the columns.

It is necessary to preliminarily analyse the dissipation capacity of the beam to column joint components that are affected by seismic actions. Accordingly, it is recommended to distinguish between dissipative and non-dissipative components, i.e., dissipative and non-dissipative failure

mechanisms [7]. With reference to joint components this distinction can be made according to Table 2.1.

Table 2.1: Dissipation capacity of single joint component [7]

	Component	Dissipative	Non-Dissipative
1	Column web panel in shear	✓	
2	Column web in compression		
	2.1 without buckling	✓	
	2.2 with buckling		✓
3	Column web in tension	✓	
4	Column flange in bending		
	4.1 welded joints		✓
	4.2 bolted joints	✓	
5	End plate in bending	✓	
6	Flange cleat in bending		
	6.1 without local buckling	✓	
	6.2 premature local buckling		✓
7	Beam web in tension	✓	
8	Plate in tension	✓	
9	Plate in compression		
	9.1 without local buckling	✓	
	9.2 premature local buckling		✓
10	Bolt in tension		✓
11	Bolt in shear		✓
12	Bolt in bearing (on beam flange, column flange, end plate or cleat)	✓	

The knowledge of the joint cyclic response and its modelling represents an essential point when the frame design is based on the dissipation of the seismic input energy in the linking elements.

Many research programs have been carried out worldwide on the cyclic response of beam to column joints to identify the behaviour parameters governing the cyclic response and at the modeling of hysteretic behaviour. Furthermore, many efforts have carried to identify low cycle fatigue [8].

Mostly research works deals with the whole joint response and its modelling. This methodology does not permit an easy identification of the contribution of each component and, as a result, of the role played by the geometrical and mechanical parameters. A different methodology can be based on the statement that the cyclic behaviour of beam-to-column joints can be predicted by properly combining the cyclic response of its basic components. This methodology represents the extension to the cyclic behaviour of the component approach widely investigated in the case of monotonic loading conditions [8].

The components governing the cyclic response of partially restrained bolted connections have been identified so that the idea of predicting the cyclic response of connections starting from the knowledge of the cyclic response of their basic components has given impetus for research, both experimental analysis and modelling, on isolated joint components [4,5,6,9]. In particular, Swanson and Leon [9] have tested 48 isolated T-stubs with the primary goal of developing design rules for T-stub joints that would result in a full strength joint, ductile behaviour and a joint stiffness close to the full restraint range. In addition, they tested also six full scale beam to column joints indicating that the T-stubs in the full scale tests performed very similarly to those tested as components.

An accurate forecast of the joint rotational performance under cyclic loads, relied on the component methodology, involves the preliminary characterization of the cyclic response of the joint components. For this reason, following dissertation dedicated to the analysis of the cyclic behaviour of the most important component of bolted joints, i.e. bolted T-stubs. In this work, analytical results are resumed and the preliminary models for predicting the cyclic response of such fundamental components are presented and discussed.

2.2. Experimental Program on Bolted T-stub under Cyclic Loads

In [8], author investigated cyclic response of T-stub under cyclic loading conditions and monotonic loading conditions on the basis of experimental tests on T- stub assemblages. In that research, author examined 28 specimens, 20 under cyclic loading conditions with constant amplitude, 4 under cyclic loading conditions with variable amplitude and 4 under monotonic loading conditions.

From 28 specimens, 7 derived from a HEA 180 profile (series HEA 180), from a HEB 180 profile (series HEB 180), 7 composed by welding with flange thickness equal to 12 mm (series W12) and 7 composed by welding with flange thickness equal to 18 mm (series W18). 1 monotonic test, 5 constant amplitude test, 1 variable amplitude test had been carried out with reference to each series of specimens.

The main objective of the monotonic tests was the investigation of plastic deformation capacity of the specimens whose values had been adopted for development of the range of the amplitude values to be used in cyclic tests. The results of all monotonic tests are presented in Figure 2.1.

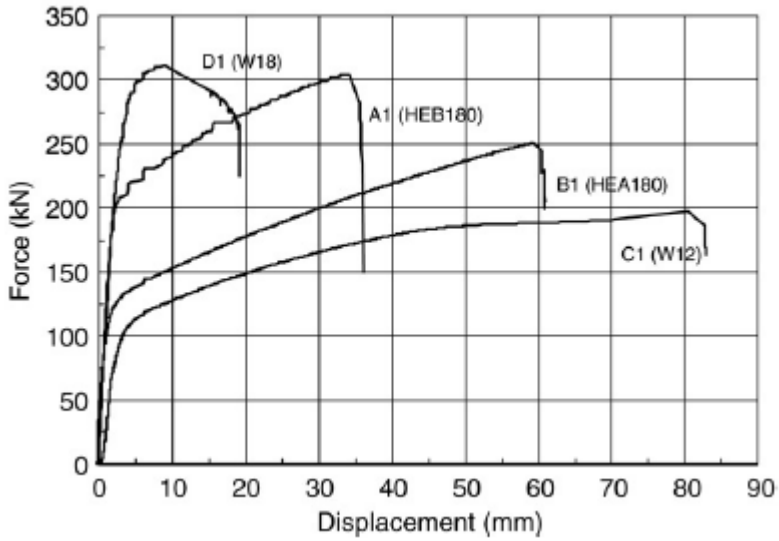

Figure 2.1: Results of monotonic tests [8]

With respect to cyclic tests, author [8] found that all specimens belonging to HEA 180 and W12 series, showed same failure mode independent of the imposed displacement amplitude. Initially formation of cracks in flanges is in the central part of flange at the flange to web connection zone the number of cycles corresponding to the development of first cracking was dependent on the displacement amplitude of the cyclic test, being as much greater as smaller is the displacement. These cracks progressively propagated toward the flange edges up to the complete fracture of one flange which causes the complete loss of load carrying capacity by increasing the number of the cycles, shown in Figure 2.2.

Figure 2.2: Failure mode of specimen under cyclic tests [8]

This type of behaviour leads to a progressive deterioration, up to failure, of axial strength, stiffness and energy dissipation capacity, as presented in Figure 2.3 and in Figure 2.4. Author [8] concluded that all aforementioned specimens showed different collapse mechanism under monotonic loading conditions and under cyclic loading conditions, where the yielding of flanges were accompanied by the bolt fracture. On the other hand, specimens belonging to HEB 180 and W 18 series, the cyclic behaviour was characterized by horizontal slips before reloading due to relevant plastic deformations of the bolts. During these slips the axial force is equal to zero up to the recovery of the bolt plastic deformation before reloading. While this type of premature failure mode was not observed in HEA 180 and W 12 series, subjected to cyclic loading.

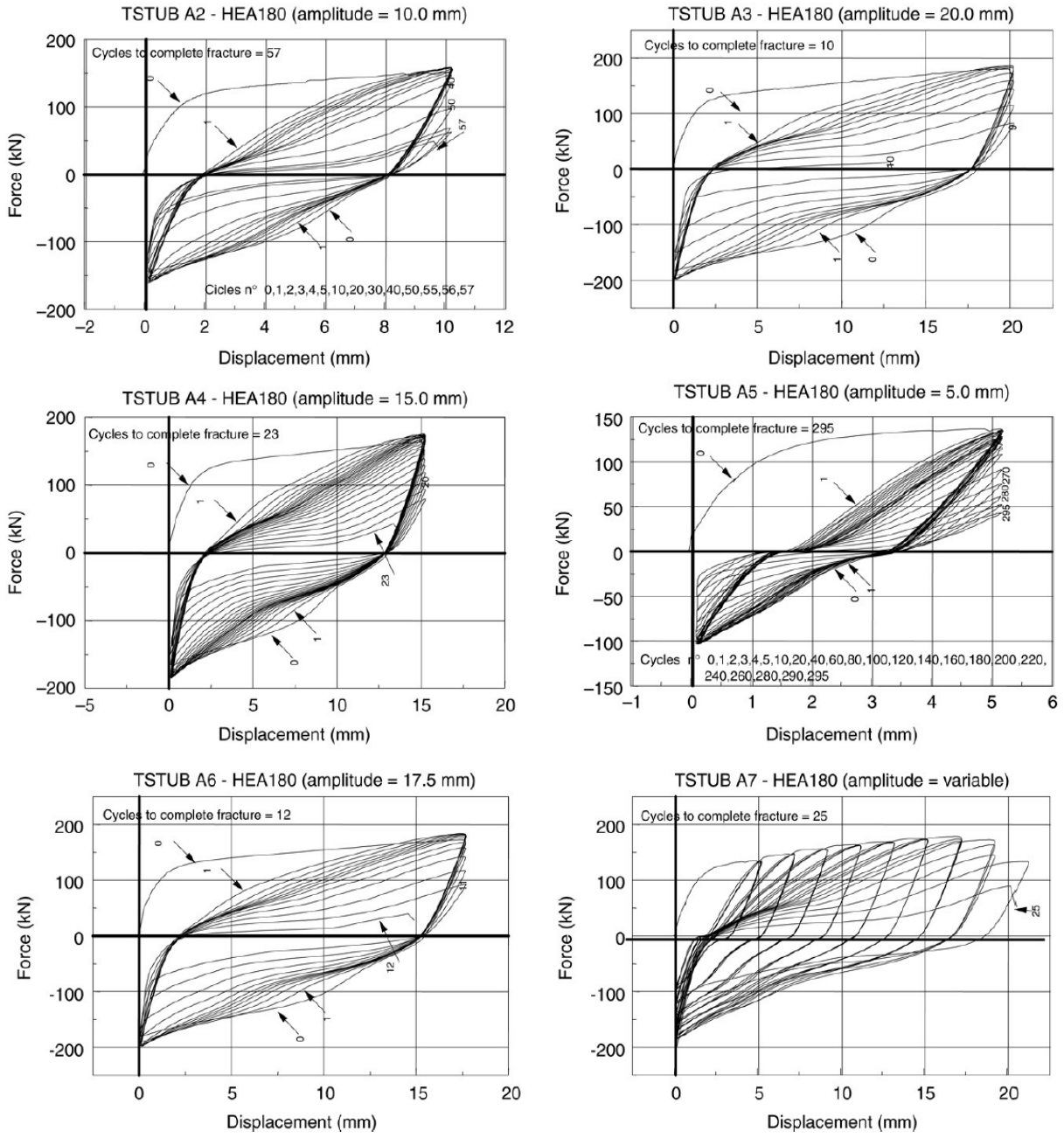

Figure 2.3: Specimen´s behaviour belonging to A series [8]

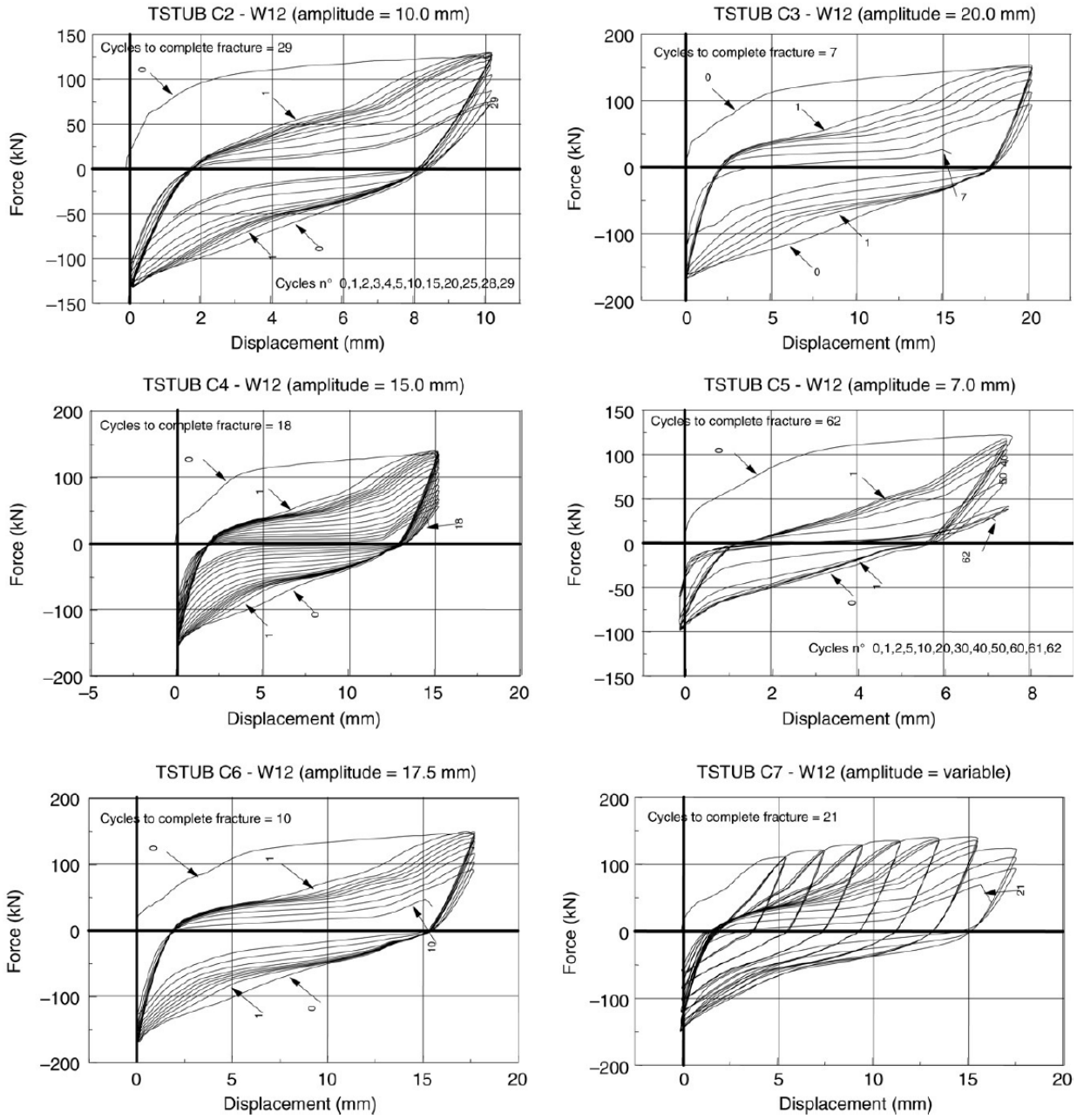

Figure 2.4: Specimen´s behaviour belonging to series C [8]

The stiffness and degradation laws had been proposed both in case of specimens failing, under monotonic loads, according to type 1 and in the case of specimens failing, under monotonic loads, according to either type 2 or type 3 failure mode by [8].

In addition, his work also proposed that, as the failure mode under monotonic loading conditions can be different from that occurring under cyclic loads, the correlation between the energy dissipation corresponding to the failure condition and the energy dissipated in monotonic conditions up to a displacement amplitude equal to that of the cyclic tests have been provided.

On the basis of the above analysis, semi-analytical models for predicting the cyclic behaviour of the T-stub assemblages starting from their geometrical and mechanical properties have been developed. Finally, the degree of accuracy of the proposed models have been pointed out by the good agreement with the experimental results in terms of energy dissipation capacity [8].

2.3. The Component Method

The component method has the prospective to predict the response of joints, whatever geometrical configuration of joint and type of member cross sections, under any loading condition (axial loading, bending or cyclic loading etc.) but for that, it is required to know the exact behaviour of each component shown in Table 2.2, see Figure 2.5. To know the behaviour of the joint it is essential to know post yield behaviour of components accounting for strain hardening effects, their ultimate resistance, their deformations ability but also the degradation of their strength and stiffness, due to cyclic loads [10].

The following steps are required for application of the component method:

1. Identification:

   Active component of concern joint should be identifying;
2. Characterization:

   Evaluation of the behaviour of each individual component;

3. Assembly:

   Assembly of all constituent components and evaluation of the behaviour of the entire beam-to-column joint.

The strength of basic components in tension or compression is usually based on an effective width (b_{eff}) while the strength of a basic component under bending or subjected to transverse forces is based on equivalent T-Stub, i.e. a geometrical idealization of T profile made of a web in tension and a flange in bending bolted by the flange [10].

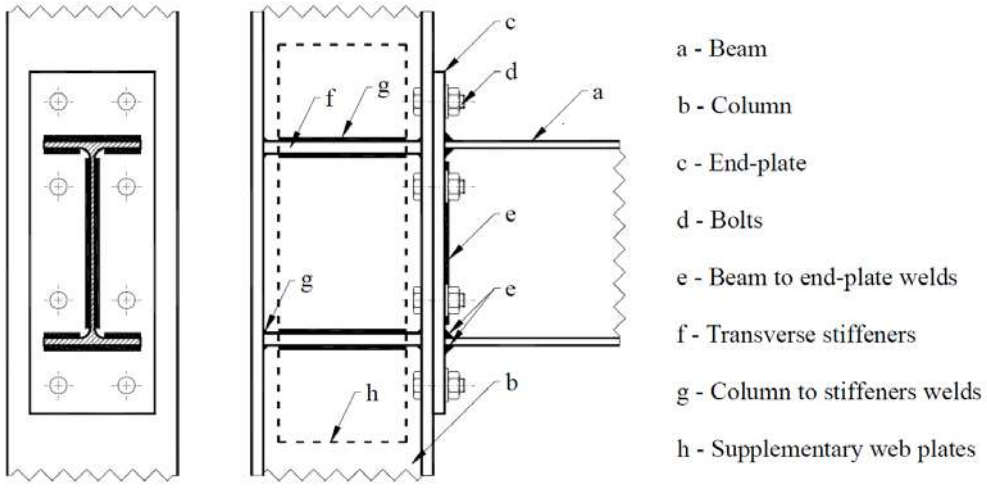

Figure 2.5: Typical beam-to-column end-plate bolted joint [11]

The component method allows to determine the bending moment resistance ($M_{j,Rd}$), the rotational stiffness (S_j) and the rotation capacity (ϕ_{Cd}), according to the scheme of Figure 2.6. The design moment resistance ($M_{j,Rd}$) is equal to the maximum moment of design moment-rotation curve, and is defined by Eq. 2.1

$$M_{j,Rd} = \sum_r h_r F_{tr,Rd} \qquad \text{Eq. 2.1}$$

where $F_{tr,Rd}$ is the effective design tension resistance of bolt-row r, h_r is the distance from bolt row r to the centre of compression and r is the bolt-row number. If the bolt-rows in tension are more

than one, then they are numbered starting from the bolt-row farthest from the centre of compression. The rotational stiffness (S_j) is a secant stiffness, moment require to produce unit rotation in a joint. For a design moment-rotation characteristic this definition of S_j applies up to the rotation ϕ_{xd} at which $M_{j,Ed}$ first reaches $M_{j,Rd}$, but not for larger rotations as shown in Figure 2.6. The initial $S_{j,ini.}$ which is slope of elastic range of the design moment-rotation characteristic. S_j is defined by *Eq. 2.2*

$$S_j = \frac{Ez^2}{\mu \sum_i \frac{1}{k_i}} \qquad \text{Eq. 2.2}$$

where E is the Young's modulus, k_i is the stiffness coefficient for basic joint component i, z is the lever arm – for two or more bolt rows an equivalent lever arm may be determined – and μ is the stiffness ratio $\frac{S_{j,ini}}{S_j}$, where $S_{j,ini}$ is given by Eq. 2.2 with μ = 1.0. The stiffness ratio μ should be determined from the following [13]:

$$\text{if} \quad M_{j,Ed} \leq \frac{2}{3} M_{j,Rd} \text{ than } \mu = 1 \qquad \text{Eq. 2.3}$$

$$\text{if} \quad \frac{2}{3} M_{j,Rd} < M_{j,Ed} \leq M_{j,Rd} \text{ than } \mu = \left(\frac{1.5\, M_{j,Ed}}{M_{j,Rd}}\right)^{\psi} \qquad \text{Eq. 2. 4}$$

The design rotation capacity ϕ_{Cd} of a joint is equal to the maximum rotation of the design moment-rotation curve [2].

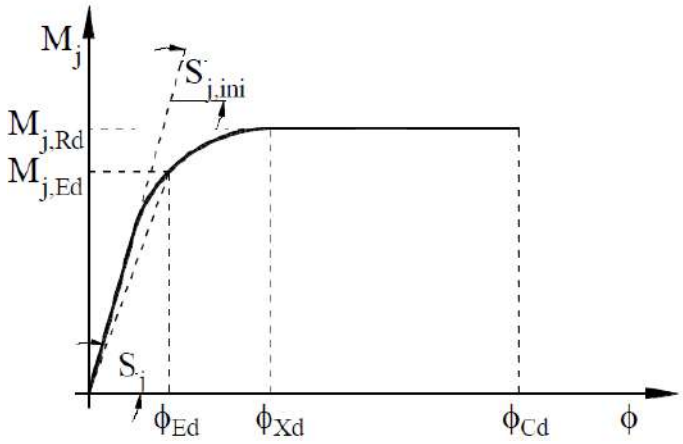

Figure 2.6: Design moment-rotation characteristics for a joint [2]

Table 2.2: List of components [2]

Sr. No	Component		Sr. No	Component	
1	Column web panel in shear	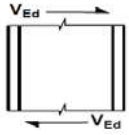	2	Column web in transverse compression	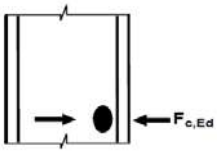
3	Column web in transverse tension	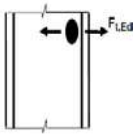	4	Column flange in bending	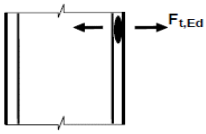
5	End-plate in bending	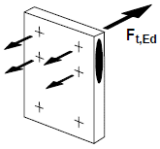	6	Flange cleat in bending	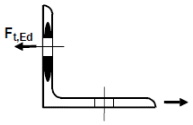
7	Beam or column flange and web in compression	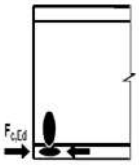	8	Beam web in tension	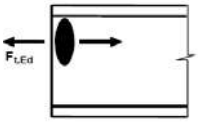
9	Plate in tension or compression	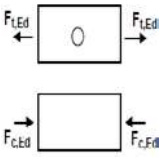	10	Bolts in tension	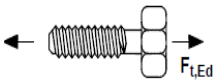
11	Bolts in shear	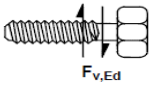	12	Bolts in bearing (on beam flange, column flange, end-plate or cleat)	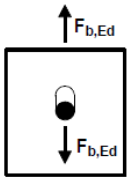

2.3.1. The T-Stub model

The assessment of the strength of the basic components involving plates subjected to transverse forces (e.g. column flange in bending, end plate in bending, flange cheat in bending and base plate in bending), according to EC3 [2] is based on a geometric idealization of the tension zone known as T-Stub. A T-stub is a T profile element made of a web in tension and a flange in bending, where the flange is assumed to be attached to a rigid foundation [10], Figure 2.7.

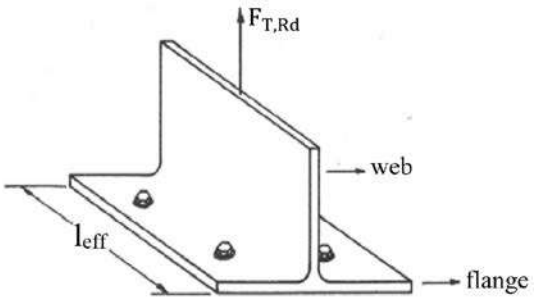

Figure 2.7: T-Stub Geometry

The equivalence between the T-stub model and the actual basic component is reached through the definition of an appropriate length of the equivalent T-Stub so-called effective length (l_{eff}) [12]. Aforementioned basic component under transvers forces may be studied with similar model and thus with similar design formulae, whatever the considered mechanical properties (stiffness, resistance or ductility) [10].

A T-stub may collapse according three different failure modes shown in Figure 2.11and Figure 2.12 (according to the geometry and the mechanical properties of the plates and the bolts) [2]:

Mode 1: Complete yielding of flange (Ductile mode)

The resistance is associated to the formation of a plastic yield mechanism in the flange. In such a case bolts are sufficiently strong to resist to the applied axial tension forces, including the praying forces Q shown in Figure 2.8.

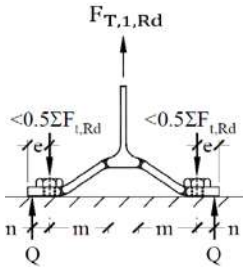

Figure 2.8: Failure mode 1 (ductile mode)

$$F_{T,1,Rd} = \frac{4\,M_{pl,1,Rd}}{m} \qquad \text{Eq. 2.5}$$

Mode 2: Bolt failure with partial yielding of the flange (Intermediate mode)

Mixed failure is achieved through the formation of yield lines the flange (the full plastic mechanism being not reached) and the failure of bolts in tension (again including prying effects), Figure 2.9.

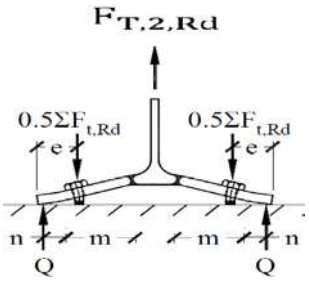

Figure 2.9: Failure mode 2 (Intermediate mode)

$$F_{T,2,Rd} = \frac{2\,M_{pl,2,Rd} + n\,\sum F_{t,Rd}}{m+n} \qquad \text{Eq. 2.6}$$

Mode 3: Bolt failure (Brittle mode)

The resistance is linked to the failure of the bolts in tension. The deformation of flange in bending is small, resulting in absence of prying effects, Figure 2.10.

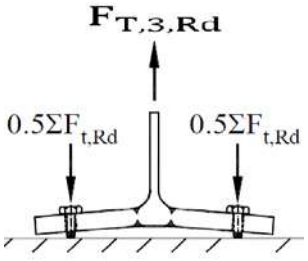

Figure 2.10: Failure mode 3 (brittle mode)

$$F_{T,3,Rd} = \sum F_{t,Rd} \qquad \text{Eq. 2.7}$$

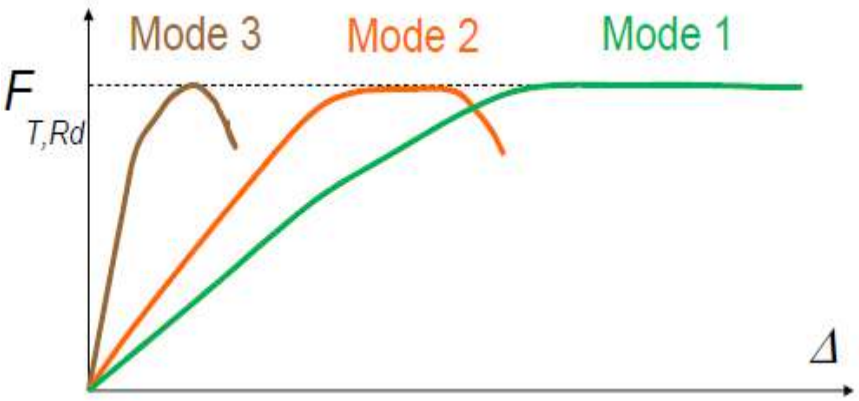

Figure 2.11: Schematic failure modes of T-Stub [13]

Figure 2.12: Ductile failure mode & Intermediate failure mode in T-Stub profiles [14]

Where;

$F_{T,Rd}$ is the design tension resistance of T-stub

Q is the prying force

$M_{pl,1,Rd}$ $= \frac{0.25 \sum l_{eff,1} t_f^2}{\gamma_{M0}}$

$M_{pl,2,Rd}$ $= \frac{0.25 \sum l_{eff,2} t_f^2}{\gamma_{M0}}$

n $= e_{min}$ but $n \leq 1.25m$

t_f is thickness of the T-Stub flange

f_y is the yield strength of the T-Stub flange

γ_{M0} is partial safety factor for the resistance of flange (recommended value: γ_{M0} = 1)

$\sum l_{eff,1}$ is value of $l_{eff,1}$ for Mode 1

$\sum l_{eff,2}$ is value of $l_{eff,2}$ for Mode 2

$\sum F_{t,Rd}$ is the sum of design resistance $F_{t,Rd} = \frac{0.9\, A_s\, f_{ub}}{\gamma_{M2}}$ of all bolts in T-Stub

A_s is the tensile stress area of the bolts

f_{ub} is the ultimate strength of the bolts

γ_{M2} is the partial resistance factor of the bolts (recommended value γ_{M2} = 1.0)

e_{min}, m and t_f are shown in Figure 2.13.

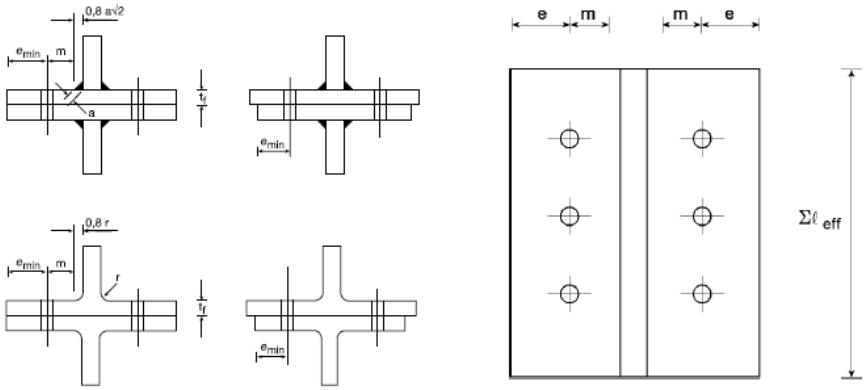

Figure 2.13: Dimensions of an equivalent T-stub flange [13]

The effective length (l_{eff}) of T-Stub depends on the geometry of T-Stub (number of bolts, stiffener probability, the distance of bolts to the edges [2]. Different values of effective length, as shown in Table 2.3 and Table 2.4 for end plate in bending and stiffened column flange in bending respectively, are linked with the following types of yield patterns: (i) individual non circular yield patterns, (ii) individual circular yield patterns, (iii) group non circular yield patterns, (iv) group circular yield patterns.

Establishment of prying forces in T-Stub leads to individual non circular yield line pattern. Depending on β values, failure mode 1, 2 or 3 may arise, as shown in Figure 2.14 where

$$\beta = \frac{4\,M_{pl,1,Rd}}{m\sum F_{t,Rd}} = \frac{Mode_{\,1}}{Mode_{\,3}} \qquad \text{Eq. 8}$$

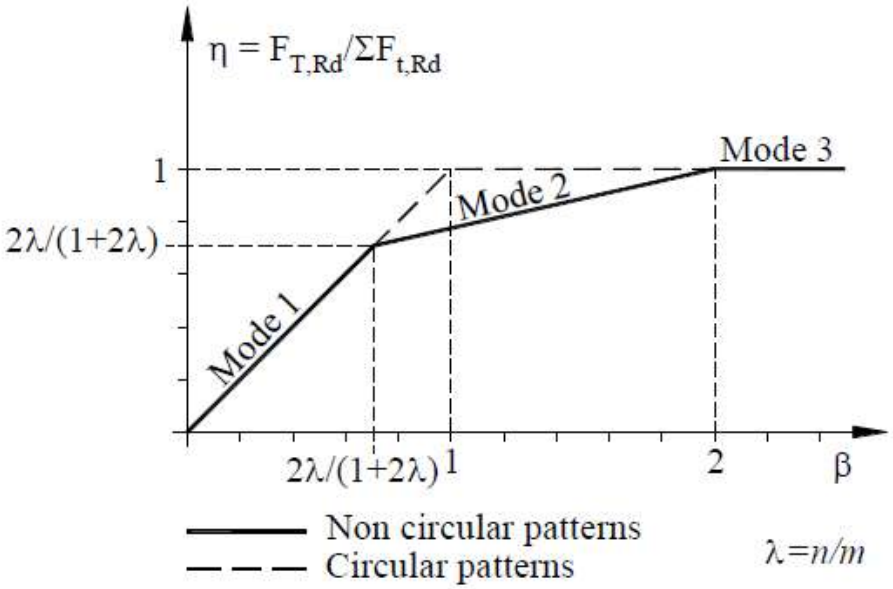

Figure 2.14: Type of failure depending on the geometry of T-Stub [2]

On the other hand, if the prying forces cannot develop in the T-Stub then individual circular yield line pattern develops. In this scenario failure mode 2 cannot occur, as shown in Figure 2.14.

Table 2.3: Effective length of end plate [2]

Bolt-row location	Bolt-row considered individually		Bolt-row considered as part of a group of bolt-rows	
	Circular patterns $\ell_{eff,cp}$	Non-circular patterns $\ell_{eff,nc}$	Circular patterns $\ell_{eff,cp}$	Non-circular patterns $\ell_{eff,nc}$
Bolt-row outside tension flange of beam	Smallest of: $2\pi m_x$ $\pi m_x + w$ $\pi m_x + 2e$	Smallest of: $4m_x + 1{,}25e_x$ $e+2m_x+0{,}625e_x$ $0{,}5b_p$ $0{,}5w+2m_x+0{,}625e_x$	—	—
First bolt-row below tension flange of beam	$2\pi m$	αm	$\pi m + p$	$0{,}5p + \alpha m - (2m + 0{,}625e)$
Other inner bolt-row	$2\pi m$	$4m + 1{,}25\,e$	$2p$	p
Other end bolt-row	$2\pi m$	$4m + 1{,}25\,e$	$\pi m + p$	$2m+0{,}625e+0{,}5p$
Mode 1:	$\ell_{eff,1} = \ell_{eff,nc}$ but $\ell_{eff,1} \le \ell_{eff,cp}$		$\sum\ell_{eff,1} = \sum\ell_{eff,nc}$ but $\sum\ell_{eff,1} \le \sum\ell_{eff,cp}$	
Mode 2:	$\ell_{eff,2} = \ell_{eff,nc}$		$\sum\ell_{eff,2} = \sum\ell_{eff,nc}$	

(α should be obtained from Figure 2.15).

Table 2.4: Effective length for stiffened column flange [2]

Bolt-row Location	Bolt-row considered individually		Bolt-row considered as part of a group of bolt-rows	
	Circular patterns $\ell_{eff,cp}$	Non-circular patterns $\ell_{eff,nc}$	Circular patterns $\ell_{eff,cp}$	Non-circular patterns $\ell_{eff,nc}$
Bolt-row adjacent to a stiffener	$2\pi m$	αm	$\pi m + p$	$0{,}5p + \alpha m - (2m + 0{,}625e)$
Other inner bolt-row	$2\pi m$	$4m + 1{,}25e$	$2p$	p
Other end bolt-row	The smaller of: $2\pi m$ $\pi m + 2e_1$	The smaller of: $4m + 1{,}25e$ $2m + 0{,}625e + e_1$	The smaller of: $\pi m + p$ $2e_1 + p$	The smaller of: $2m + 0{,}625e + 0{,}5p$ $e_1 + 0{,}5p$
End bolt-row adjacent to a stiffener	The smaller of: $2\pi m$ $\pi m + 2e_1$	$e_1 + \alpha m - (2m + 0{,}625e)$	not relevant	not relevant
For Mode 1:	$\ell_{eff,1} = \ell_{eff,nc}$ but $\ell_{eff,1} \le \ell_{eff,cp}$		$\sum\ell_{eff,1} = \sum\ell_{eff,nc}$ but $\sum\ell_{eff,1} \le \sum\ell_{eff,cp}$	
For Mode 2:	$\ell_{eff,2} = \ell_{eff,nc}$		$\sum\ell_{eff,2} = \sum\ell_{eff,nc}$	

(α should be obtained from Figure 2.15).

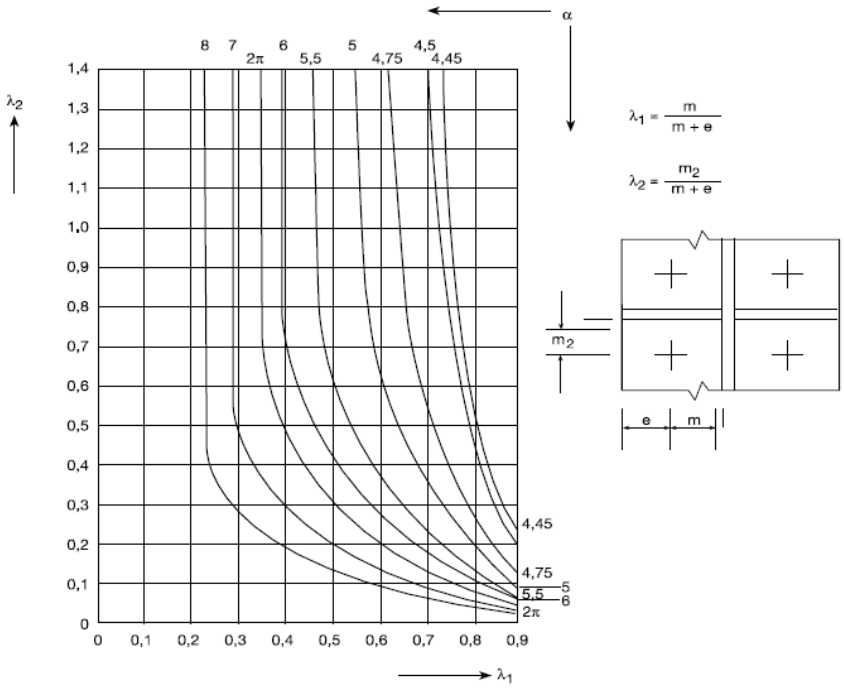

Figure 2.15: Values of α for stiffened column flanges and end-plates [2]

According to the latter considerations, the resistance of T-Stub will be

$$F_{T,Rd} = \min (F_{T,1,Rd}; F_{T,2,Rd}; F_{T,3,Rd}) \quad \text{Eq. 2.9}$$

for non-circular patterns and

$$F_{T,Rd} = \min (F_{T,1,Rd}; F_{T,3,Rd}) \quad \text{Eq. 2.10}$$

for circular patterns.

3. Finite Element Modeling (FEM)

The finite element method (FEM), sometimes refers to a finite element analysis (FEA), is a powerful tool for computation of complex problems, used to obtain approximate numerical solutions. FEM is appropriate to problems throughout continuum mechanics, applied mathematics, engineering, and physics [15].

3.1. FEM elements in ABAQUS

In this dissertation, to assess the cyclic behaviour of stiffened column flange in bending, finite element models were developed in ABAQUS software, version 6.14 [16]. These models aimed to perform a parametric analysis to assess the influence of the collapse mode in the cyclic behaviour of this basic component.

A wide range of variety of elements are used in ABAQUS software for different modelling analysis. The types of elements available in ABAQUS will be briefly addressed taking into account the following features [16];

- Family
- Degree of freedom (directly related to element family)
- Number of nodes
- Formulation
- Integration

Each type of element contains a unique name in ABAQUS software such as T2D2, S4R, or C3D8I. The elements name classifies aforementioned aspect of an element [16].

3.1.1. Family

One of major distinction between different element families is the geometry type of the elements. The first letter/letters of an element identify the family that the elements belong, e.g. the C in C3D8I exhibits this is a continuum element however, the S in S4R exhibits this is a shell element. Following are commonly used element families, as shown in Figure 3.1.

Continuum (solid) elements

- Shell elements
- Beam elements
- Rigid elements
- Membrane elements
- Infinite elements
- Spring and dashpots
- Truss elements

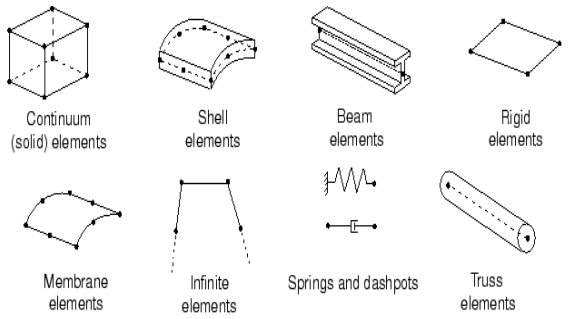

Figure 3.1: Element families in ABAQUS software [16]

3.1.2. Degrees of freedom

The degrees of freedom (DOF) are the fundamental variables which are considered during the resolution of the equilibrium equations. For a stress/displacement analysis, the degrees of freedom are the translations at each node of each element. Some element families, such as the beam and shell families, may also have rotational degrees of freedom as well.

3.1.3. Number of nodes (Order of interpolation)

Rotation, displacement, temperature, and other quantities are evaluated only at integration points of the element. At any other point in the element, these quantities can be obtained from the integration points through interpolation. Interpolation order is defined by the order of the polynomial shape functions used for the interpolation, as shown in Figure 3.2.

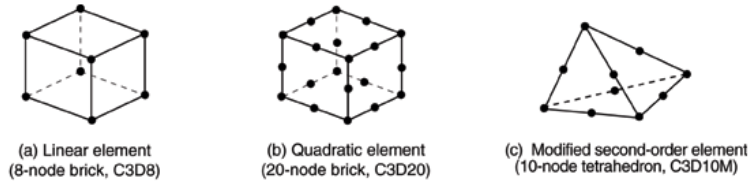

Figure 3.2: Linear brick, quadratic brick, and modified tetrahedral element [16]

3.1.4. Formulation

An element's formulation denotes to the mathematical theory used to describe the response of an element. In the absence of adaptive meshing all of the stress/displacement elements in ABAQUS are based on the Lagrangian or material description of behavior: the material linked with an element remains linked with the element during the analysis, and material cannot flow across element boundaries. In the alternative *Eulerian* or *spatial* description, elements are fixed in space as the material flows through them. Eulerian methods are used commonly in fluid mechanics simulations. ABAQUS/Standard uses Eulerian elements to model convective heat transfer. Adaptive meshing combines the features of pure Lagrangian and Eulerian analyses and allows the motion of the element to be independent of the material [16].

To accommodate different types of behavior, some element families in ABAQUS include elements with several different formulations. For example, the shell element family has three classes: one suitable for general-purpose shell analysis, another for thin shells, and yet another for thick shells.

Some ABAQUS/Standard element families have a standard formulation as well as some alternative formulations. Elements with alternative formulations are identified by an additional character at the end of the element name. For example, the continuum, beam, and truss element families include members with a hybrid formulation in which the pressure (continuum elements) or axial force (beam and truss elements) is treated as an additional unknown; these elements are identified by the letter “H” at the end of the name (C3D8H or B31H).

Some element formulations allow coupled field problems to be solved. For example, elements whose names begin with the letter C and end with the letter T (such as C3D8T) possess both mechanical and thermal degrees of freedom and are intended for coupled thermal-mechanical simulations.

Several are of the most commonly used elements formulation are described in ABAQUS documentation.

3.1.5. Integration

ABAQUS software uses numerical system to integrate various quantities over the volume of each element. ABAQUS evaluates the material response at each integration point in each element. Some elements can use full or partial integration.

ABAQUS uses the letter “R” at the end of the element name to discriminate reduced-integration elements (unless they are also hybrid elements, in which case the element name ends with the letters “RH”), shown in Figure 3.3. For example, CAX4 is the 4-node, fully integrated, linear, axisymmetric solid element; and CAX4R is the reduced-integration version of the same element.

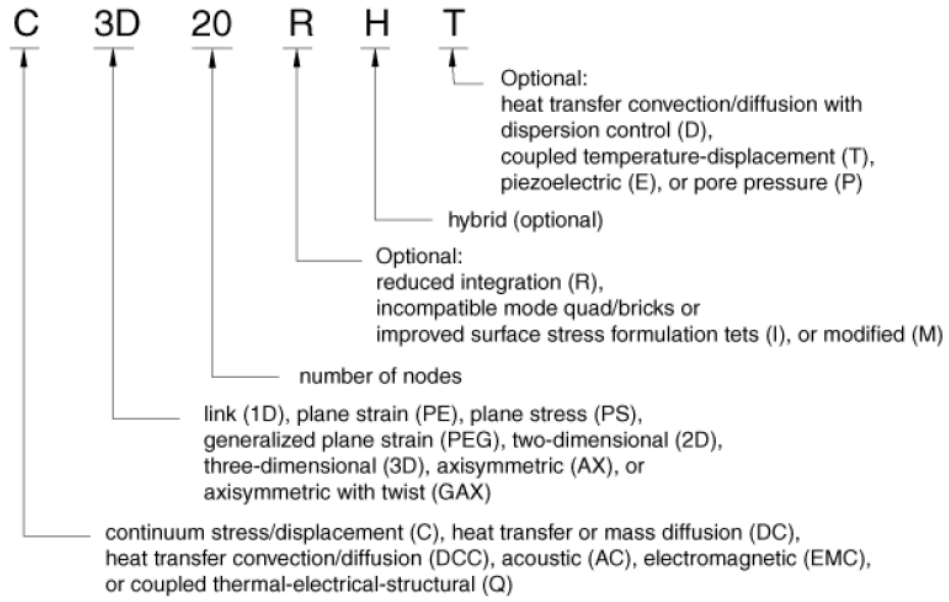

Figure 3.3: Naming convention of solid elements in ABAQUS [16]

3.2. Solid Elements

The solid (or continuum) elements will be used in this dissertation. These elements are recommended for complex linear or nonlinear analysis involving contact, plasticity and large deformations.

3.2.1. Choosing between quadrilateral and tetrahedral mesh element shapes

With tetrahedral mesh elements it is easy to mesh large complex forms. ABAQUS provides automatic meshing algorithmic which makes it easy to mesh very complex geometry. Tetrahedral mesh elements are therefore more suited to mesh complex geometries. However, quadrilateral mesh element type provides solutions of equal accuracy and at less computer cost. Quadrilateral mesh elements are more efficient in convergence than tetrahedral mesh elements. Quadrilateral mesh elements perform better if their shapes are approximately rectangular however tetrahedral mesh elements don't depend on initial element geometry.

3.2.2. Choosing between first-order and second-order elements

Second-order elements have higher accuracy in ABAQUS/Standard than first-order elements for problem solutions that do not involve complex contact conditions, impact, or severe element alterations. Second order elements capture stress concentrations more efficiently and are better for modelling structures with complex geometries. First-order triangular and tetrahedral elements should be avoided in stress analysis problem solution because of the overly stiff nature of elements.

3.3. Material Model in FEM

In this dissertation, for steel profiles including HEA 300, bending plate and stiffener, S420 material is used while different bolt classes were used. Nominal properties were obtained from EC 3. The remainder assumed mechanical properties are shown in Table 3.1, Table 3.2, and Table 3.3.

Table 3.1: Elastic properties of material

Density	7.85×10^{-9}	$tons/mm^3$
Young's modulus	210000	N/mm^2
Poisson ratio	0.3	-

Table 3.2: Plastic properties of material for mild steel

Material	f_y (N/mm^2)	f_u (N/mm^2)	ε_y	ε_u
S 420	420	520	0.02	0.15

Table 3.3: Plastic properties of material for bolts.

Material	f_y (N/mm^2)	f_u (N/mm^2)	ε_y	ε_u
10.9	900	1000	0.02	0.15
8.8	640	800	0.02	0.15
6.8	480	600	0.02	0.15

The material model used for steel in ABAQUS was an elastic-plastic material with isotropic hardening and associative flow rule. The input for this material model required by ABAQUS is the uniaxial stress-strain relation.

Since ABAQUS will incorporate the reduction in area by itself due to the Poisson effect, True Stress-True Strain relations for uniaxial behaviour of steel are required. The stress-strain relation gathered from coupon tests are valid up to the necking point, after which the materials seems to soften but it actually hardens because of the fact that after necking significant reduction in cross-sectional area takes place which results in reduction in material resistance hence the stress values goes down but actually material continues hardening till fracture.

True Stress-True Strain relations were computed from the engineering stress-strain relations shown in Figure 3.4 through (Eq. 3.1) and (Eq. 3.2) from EN 1993-1-5. The plastic strain was computed using Eq. 3.3, where "σ_{true}" true stress, "ε_{true}" true strain, "σ_{engg}" engineering stress, "ε_{engg}" engineering strain, "ε_{pl}" plastic strain and "E" slope of linear elastic range

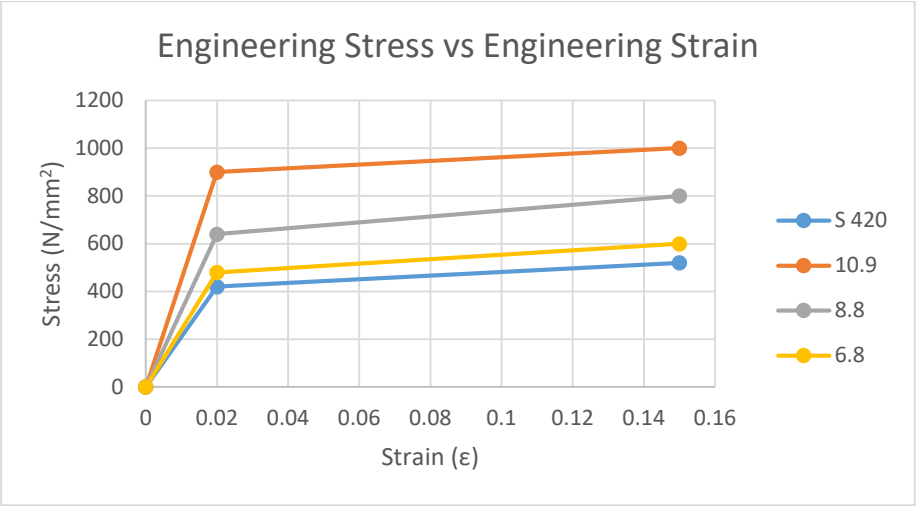

Figure 3.4: Stress vs strain

$$\sigma_{true} = \sigma_{engg} (1+ \varepsilon) \qquad \text{Eq. 3.11}$$

$$\varepsilon_{true} = \ln (1+ \varepsilon_{engg}) \qquad \text{Eq. 12}$$

$$\varepsilon_{pl} = \ln (1+ \varepsilon_{engg}) - \frac{\sigma true}{E} \qquad \text{Eq. 13}$$

Aforementioned formulas were used up to the maximum load. After the maximum load of engineering stress, the curve was considered ascending till fracture.

3.4. Constrain and Contact Interaction

In ABAQUS, different components of model interact with each other by continuity links so-called constraints (e.g. between beam flange and the end plate) or defining contact properties so-called interactions (e.g. between the end plate and column flange, between bolts and the end plate or column flange).

The beam flange elements and stiffener elements were constrained to the end plate and column respectively by a “tie constraint” that use the concept of master and slave nodes to define the same degree of freedom between both. The column edges elements were constrained with reference points for supports by “coupling constraint”, using same master and slave philosophy, the degrees

of freedom of the dependent nodes are eliminated; the two surfaces will have the same values of their degrees of freedom.

The interaction between the end plate and column flange, and the interaction between bolts and the column flange or the end plate were imposed by the general contact algorithm, which used "hard contact" formulation, using the penalty method to approximate the hard pressure overclosure behaviour (normal behaviour) that acts in the normal direction to resist penetration. Friction coefficient 0.2 was used to imposed "Tangential behaviour".

ABAQUS divides the problem history into steps. A step is any convenient phase of the history and, in its simplest form, a step can be just a static analysis, a load change from a magnitude to another, an initial pre-stress operation of a part of the structure or the change of a boundary condition in the model.

In this particular case, the solution of the problem is obtained in 3 steps. The first step is used to formulate the boundary conditions and prepare the contact interactions defined previously.

The second step corresponds to the pre-loading of the bolts using the adjust length option and determining the length magnitude by the elastic elongation needed to produce the required amount of force in the bolts, normally a percentage of the ultimate strength. Figure 3.5 shows the plane where the adjust length option is applied.

In the third step the bolts current length is fixed so the magnitude is computed during the analyses. This option allows maintaining the pre-defined load in the bolts during the third step. It is in the third step that the pushover begins, changing the boundary conditions on the tip of the cantilever by imposing a displacement in the boundary condition parallel to the beam web.

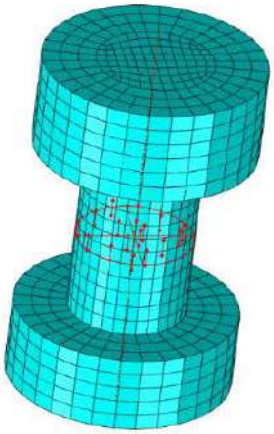

Figure 3.5: Bolts pre-loading plane [11]

3.5. Loading

The models were loaded following protocol which consisted of an imposed displacement applied at the beam flange end, according to scheme shown in Figure 4.5. All models were prepared to deal with monotonic loads and cyclic loads. The “loads” were applied in a displacement control approach, i.e. a displacement is imposed at the tip of beam flange, see Figure 4.5. The loading protocol is defined by the direction (along the three global axis, although in this dissertation only the YY axis direction was used), with same orientation but for cyclic loads, amplitude of the displacement and number of cycles are detail discussed in next chapter.

4. Numerical Model

4.1. Simplified Model Geometry and Boundaries

In order assess rigorously the internal forces transmitted to the column flange in bending instead of modelling the entire beam-to-column joint only the tension region of the joint was modelled and the beam web was not considered either, see Figure 4.1.

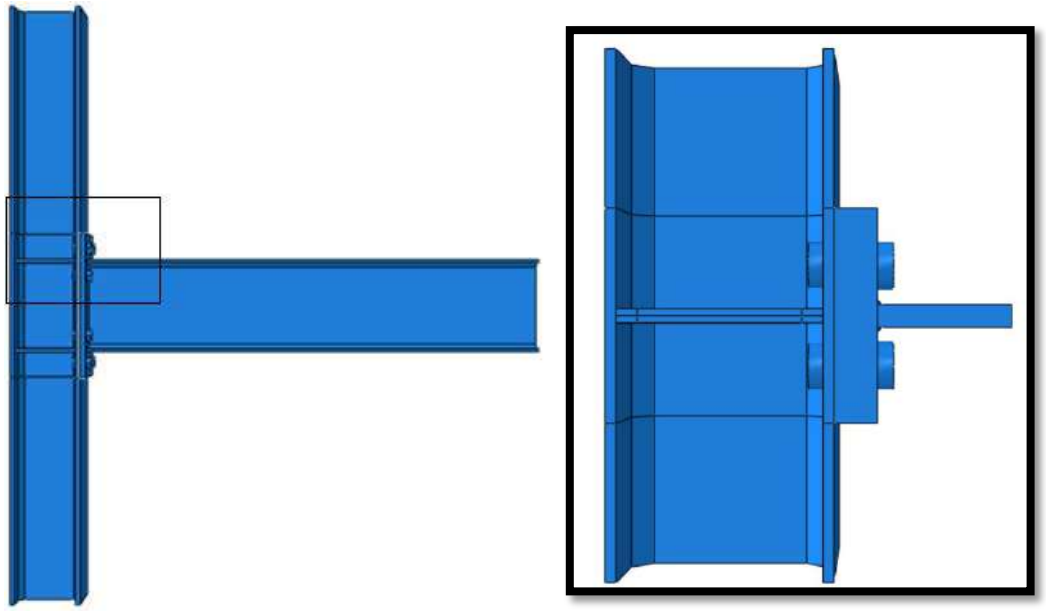

Figure 4.1: Tension part of beam-to-column joint

The analytical program, herein presented, consists in the analysis of the cyclic behaviour of the components namely, according to EC 3, “column flange in bending”, “end plate in bending” and “bolts in tension”. However, the results are obviously of concern for T-stub connections which are not directly covered by EC 3.

To predict the response of T-stub of column flange under cyclic loading, four models were constructed on ABAQUS software 6.14, based on “β”, which is ratio of failure mode 1 to failure mode 2. Bolt grades were changed from 10.9 to 6.8 and in one model bolt size was decreased from

M36 to M30 with grade 10.9 to achieve different mode ratios. Whole model is consisting of column profile (HEA 300), bending plate, stiffeners, and bolts, see in Figure 4.2.

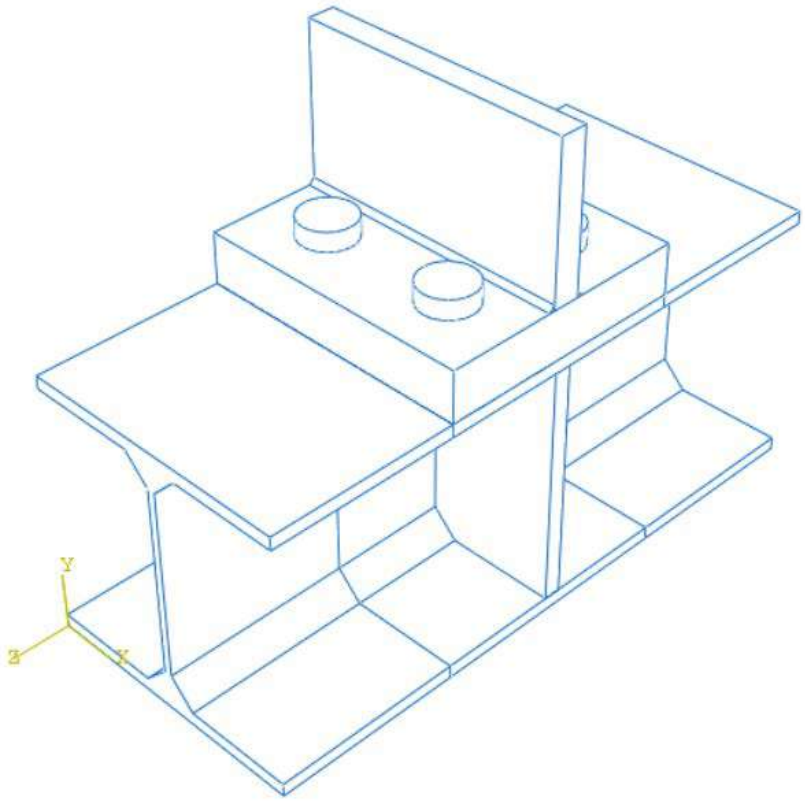

Figure 4.2: 3D view of the tension region of the beam-column joint

4.2. Parametric Analysis

The parametric analysis performed aimed to assess the influence of the ratio between the mode 1 and mode 2 of the failure loads of the T-stub corresponding of column flange in bending according to EC 3-1-8 model. Accordingly, a ratio β was considered

$$\beta = \frac{F_{T,1}}{F_{T,2,}} \qquad \text{Eq. 14.1}$$

where $F_{T,1}$ and $F_{T,1}$ were computed using expressions Eq. 2.5 and Eq. 2.6, respectively. Bolt grades were changed from 10.9 to 6.8 and in one model bolt size was decreased from M36 to M30 with grade 10.9 to achieve different mode ratios. Whole model is consisting of column profile (HEA 300), bending plate, stiffeners, beam flange and bolts, see Figure 4.2.

The models were also defined in order that the failure mode 3 in column flange in bending is always higher than the lower of failure modes 1 and 2. The end plate thickness and the beam flange was also defined to be strong enough to avoid failure modes 1 and 2 in the end plate as well as in the beam flange in tension.

4.3. FEM Model Construction

A brief description of model construction in ABAQUS is presented in the following sections together with some more details about the models.

4.3.1. Part Module

In this module, geometry of each part of the model was defined independently using the measures provided in Figure 4.3. the model comprises 5 parts that were drawn independently using the procedure shown in Table 4.1.

Table 4.1: Description of the procedures used to draw the parts of the model.

Modelling space		3D
Type		Deformation
Base feature	Shape	Solid
	Type	Extrusion

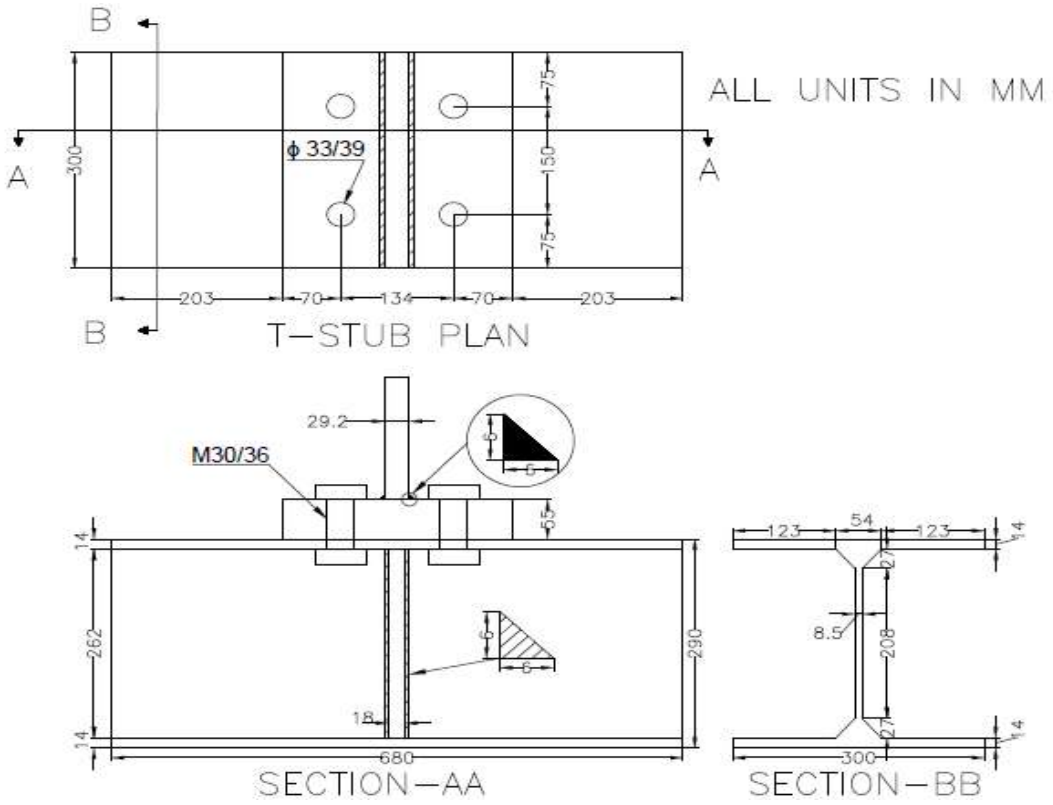

Figure 4.3: Geometrical description of the components

4.3.2. Property Module

In property module, the material model described in section 3.3 are assigned to each part of the model according to Table 4.2.

Table 4.2: Material assigned to the parts of the model

Material properties	Component of the model
S 450	HEA 300 End plate
10.9 Grade	M36/M30
8.8 Grade	M36
6.8 Grade	M36

Elastic and plastic properties of material were also introduced in this module, discussed in previous chapter.

4.3.3. Assembly Module

Each component´s geometry was defined independently, for the assembly of T-stub components, this module was used, shown in following Figure 4.4.

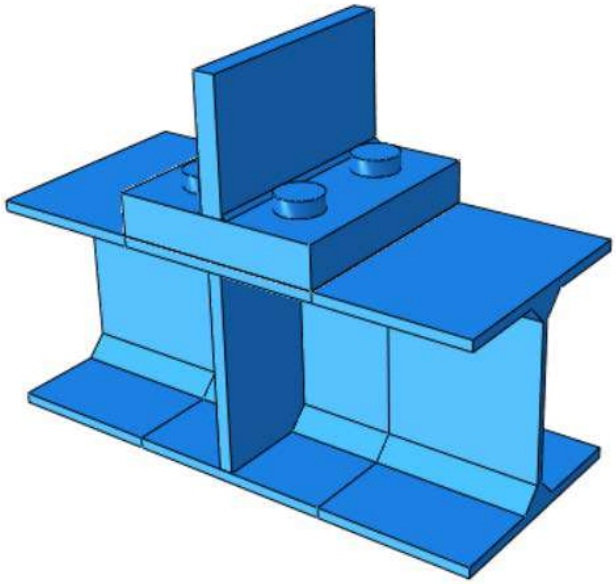

Figure 4.4: Description of assembly module of a model.

4.3.4. Step Module

Standard general-static step was used to analysis the response of T-stub under monotonic loading condition and cyclic loading condition.

History output request manager used to identify force and displacement at a specific point in beam flange.

ABAQUS divides the problem history into steps. A step is any convenient phase of the history and, in its simplest form, a step can be just a static analysis, a load change from a magnitude to

another, an initial pre-stress operation of a part of the structure or the change of a boundary condition in the model.

In this particular case, the solution of the problem is obtained in 3 steps. The first step is used to formulate the boundary conditions and prepare the contact interactions defined previously.

The second step corresponds to the pre-loading of the bolts using the adjust length option and determining the length magnitude by the elastic elongation needed to produce the required amount of force in the bolts, normally a percentage of the ultimate strength. Figure 3.5 shows the plane where the adjust length option is applied.

In the third step the bolts current length is fixed so the magnitude is computed during the analyses. This option allows maintaining the pre-defined load in the bolts during the third step. It is in the third step that the pushover begins, changing the boundary conditions on the tip of the cantilever by imposing a displacement in the boundary condition parallel to the beam web.

4.3.5. Interaction Module

The models were comprised of many parts presented in Figure 4.2, those parts were interacted with each other through constraints and/or interactions.

For bolt to steel surface (end plate and HEA 300) and end plate to HEA 300, general contact was used with friction coefficient of 0.2 in tangential behaviour and hard contact was used for specifying normal behaviour in contact property option.

Coupling and tie constraints were adopted for boundaries definition and welded parts (beam flange to end plate and stiffener to column profile) respectively.

Three reference points were selected from model and were coupled using kinematic coupling type with all degree of freedom constrained with surface of T-stub, shown in Figure 4.5.

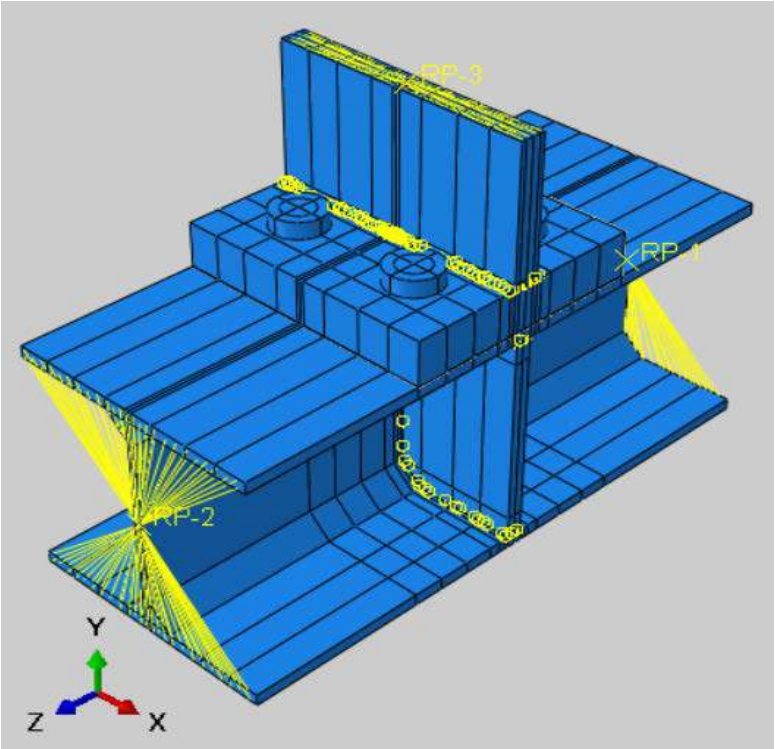

Figure 4.5: Description of interaction module of a model.

4.3.6. Load Module

The reference points RP1 and RP2 were restrained using displacement/rotation boundary type with all the displacements and rotation fixed. The reference point RP3 was allowed to have a uniform displacement along the Y-axis of the model, see Figure 4.6.

The displacement in RP3 was increased monotonically until failure of the model for monotonic loading condition. For cyclic loading condition the loading protocol presented in section 4.4 was imposed in RP3.

To minimize the lack of convergence issues encountered a preload was assign to the bolts detail discussed in 3.4 section.

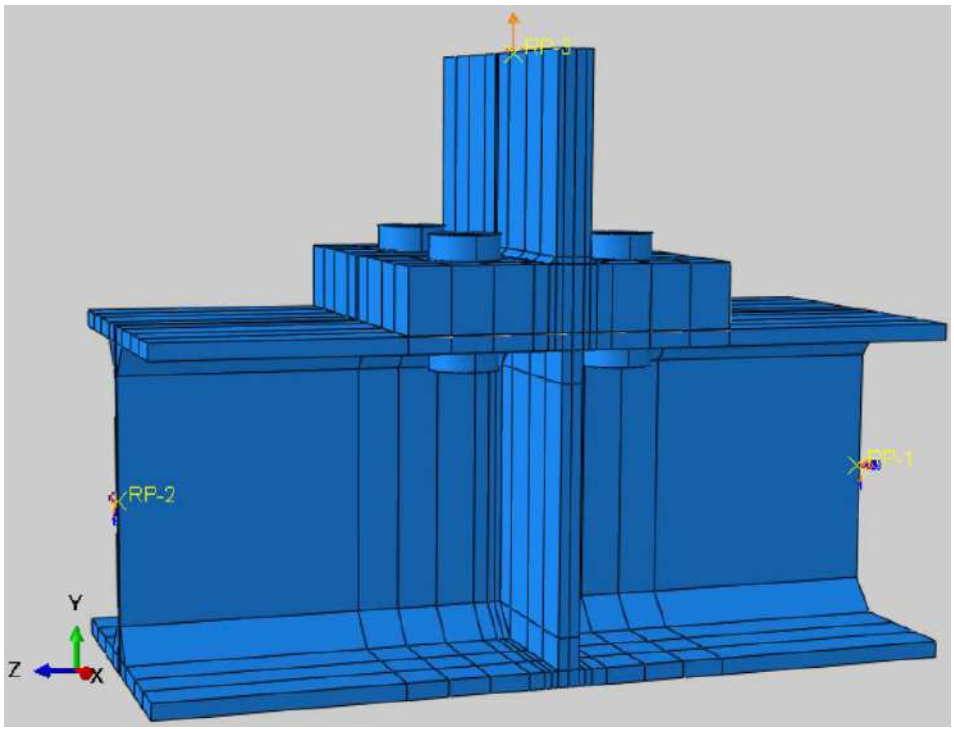

Figure 4.6: Description of load module of a model.

4.3.7. Mesh Module

The C3D8R linear brick element with 8-node, reduced integration, hourglass control of the ABAQUS element library was used for meshing all of the components of the models. To overcome the hourglass issue at least 2 layers were considered in the thickness of the end plates and column flanges of the models, shown in Figure 4.7. Approximate global size of 10 mm [11], was used for all components but around bolt holes, mesh size was reduced to avoid convergence problems. Figure 4.7 shows the meshes used in all the parts of the model

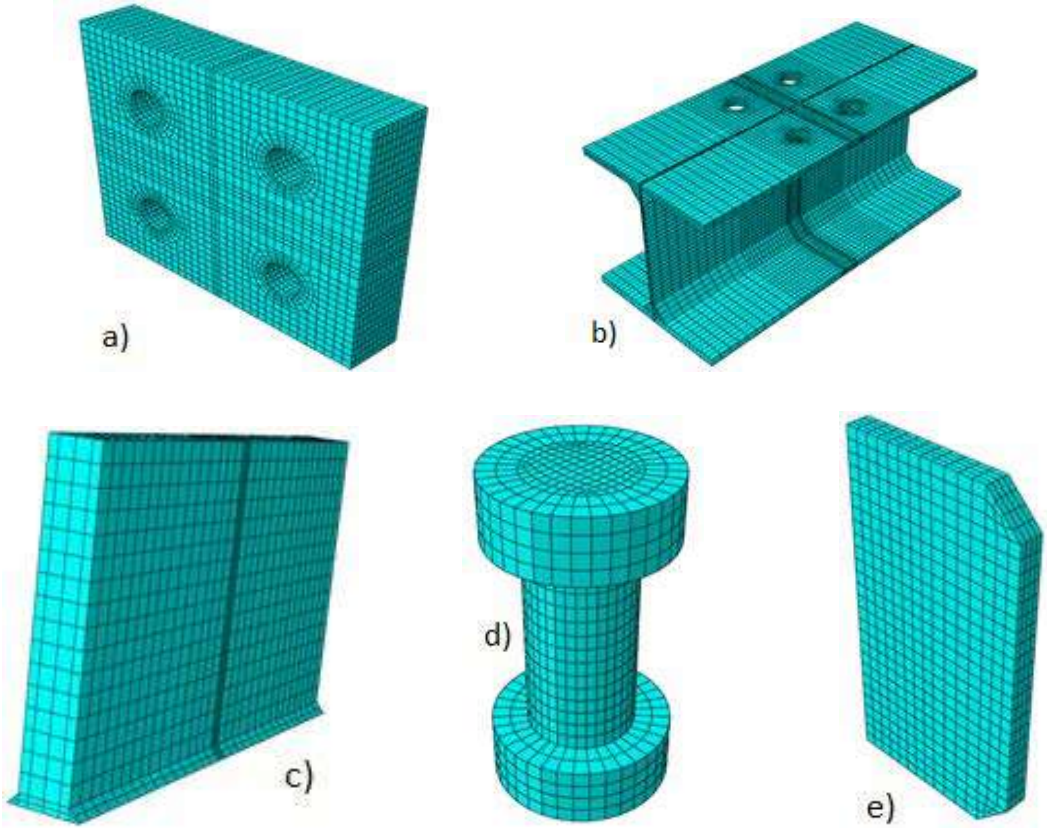

Figure 4.7: FEM mesh of the parts of the model, a) end plate, b) HEA 300, c) beam flange, d) bolt, and e) stiffener

4.3.8. Visualization Module

The visualization module was used for getting response of the models. Equivalent plastic strain (PEEQ) and maximum stress (S, Mises) provided by ABAQUS are shown in Figure 4.8 and Force - Displacement relationship is shown in Figure 4.9.

.

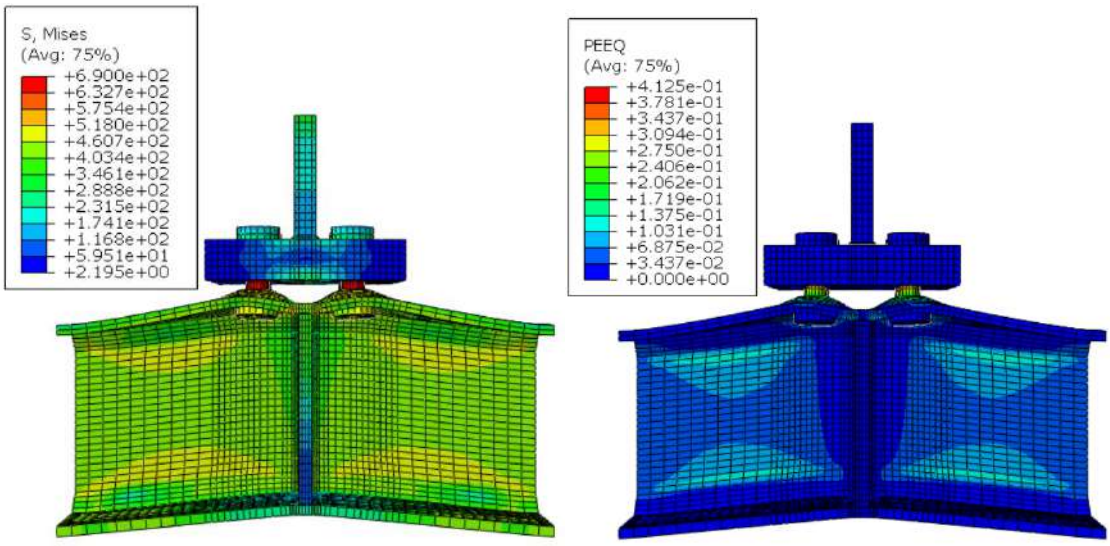

Figure 4.8: Von Misses stresses and equivalent plastic strains visualization in visualization module of ABAQUS.

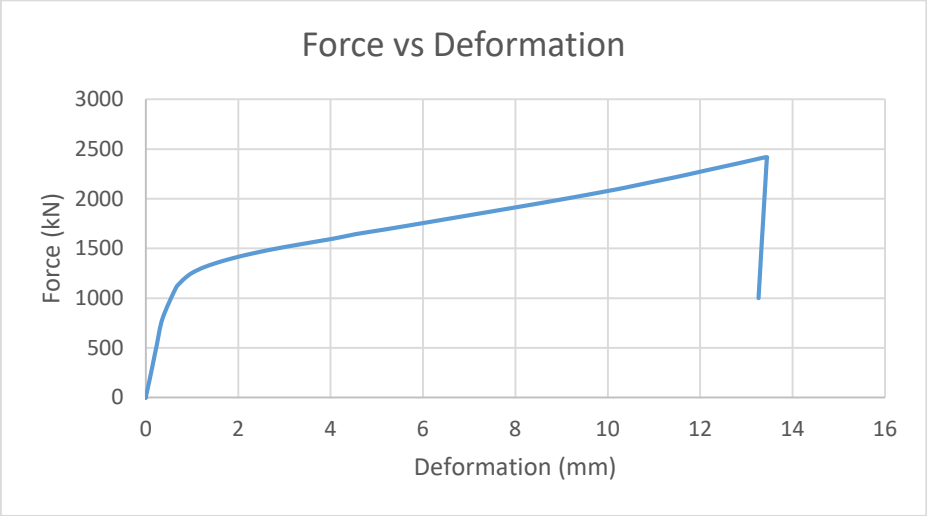

Figure 4.9: Force displacement curve in visualization module of ABAQUS

4.2. Loading Protocol

For computation of cyclic behaviour of joints in MRFs, quasi-static loading protocol has been defined in the EQUALJOINTS project in terms of interstorey drifts. These drifts were computed based in drift demands from nonlinear time history analyses of moment resisting frames (MRFs),

dual eccentrically braced frames (D-EBFs) and dual concentrically braced frame (D-CBFs) typologies [3]. The simplified protocol is given in Table 4.3.

Table 4.3: Simplified loading protocol [3]

no. of cycles	drift angle θ (rad)
6	0.004
6	0.006
4	0.010
2	0.015
2	0.020
2	0.030
2	0.040

The protocol can be continued after the maximum cycle of 0.040 rad by further loading at increments of 0.01 rad, with two cycles of loading at each step, as long as the state of the specimen permit.

Assuming in the safe side that [3]:

(i) The entire drift arises from the connection, i.e. the beam and columns are rigid and there is no deformation in the CWS;
(ii) The connection internal arm is "z" (assume it to be equal to the distance between the beam flange centerlines; 435.4 mm);
(iii) Compression components deformation is negligible (compression components are much stiffer than the tensile components);

The relation between the maximum drift angle (θ) and the deformation in the tension components (δ) is $\delta = z \times \tan(\theta)$ and the compression deformation is null. Accordingly, the load quasi static load protocol to is considered in Table 4 4 and is represented in Figure 4.10.

Table 4 4: Loading protocol for the T-stub [3]

no. of cycles	maximum tensile deformation z (m)
6	z × tan(0.004)
6	z × tan(0.006)
4	z × tan(0.010)
2	z × tan(0.015)
2	z × tan(0.020)
2	z × tan(0.030)
2	z × tan(0.040)

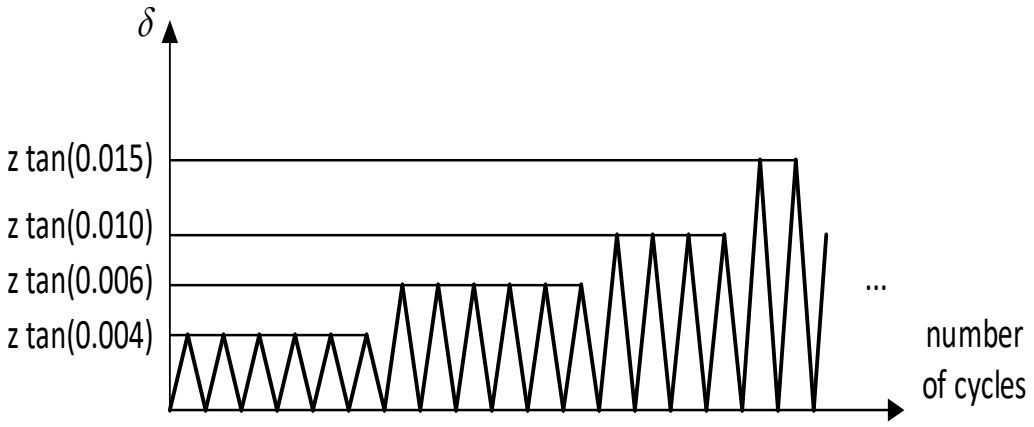

Figure 4.10: Loading protocol for a T-stub [3]

5. Results and Discussion

In this section, the full details about the models are provided and the monotonic and cyclic analysis of their behaviour and the column flange in particular is presented.

5.1. FEM Models Definition

Four models were built in ABAQUS for different values of β for column flange in bending in the range [0.75;1.25]. These models were obtained by changing the material and geometrical properties of bolts.

Having into account the EC3-1-8 provisions presented in section 2.3.1, for the geometry represented in Figure 4.3, only plastic collapse mechanism for individual bolts are possible and thus for the computation of the effective length of the T-stub the bolts need only to be considered individually – with circular and non-circular patterns for the yield lines. Accordingly, Table 5.1 presents the effective length for the column flange in bending.

Table 5.1: Effective length for a stiffened column flange in a bolted connection.

Bolt row location	Bolt row considered individually	
	Circular patterns $l_{eff,\,cp}$ (mm)	Non circular patterns $l_{eff,\,nc}$ (mm)
Bolt row adjacent to a stiffener	$2\pi m$	αm
	274.89	262.5
For Mode 1:	$l_{eff,\,1} = l_{eff,\,nc}$ but $l_{eff,\,1} \leq l_{eff,\,cp}$	262.5
For Mode 2:	$l_{eff,\,2} = l_{eff,\,nc}$	262.5
m = 43.75 mm	e_1 = 75 mm m_2 = 52 mm λ_1 = m/(m+e) 0.4	α = 6

Tables 5.3, 5.4, 5.5 and 5.6 present the mechanical properties and the bolt sizes for the models considered in the parametric analysis. These tables also present the strength of these models for the three collapse modes considered in EC3-1-8 for the T-Stub model.

Table 5.2: Strength of column flange in bending - model 1.

$\sum l_{eff,1}$ =	1050	mm	f_{ub} =	1000	N/mm^2
$\sum l_{eff,2}$ =	1050	mm	d_b =	36	mm
t_f =	14	mm	A_s =	1017.36	mm^2
f_y =	420	N/mm^2	bolts no.=	4	
m =	43.75	mm	γ_{M2} =	1	
e_1 = n =	75	mm	k_2 =	0.9	
γ_{M0} =	1				
$M_{pl1,Rd}$ =	21.61	kNm	$F_{t,Rd}$ =	915.624	kN
$M_{pl2,Rd}$ =	21.61	kNm	$\sum F_{t,Rd}$ =	3662.496	kN
$F_{T,1,Rd}$ =	1975.68	kN			
$F_{T,2,Rd}$ =	2677.10	kN			
$F_{T,3,Rd}$ =	3662.50	kN			
$F_{T,Rd}$ =	1975.68	kN	β =	$F_{T,1,Rd} / F_{T,2,Rd}$ =	0.74

Table 5.3: Strength of column flange in bending - model 2.

$\sum l_{eff,1}$ =	1050	mm	f_{ub} =	800	N/mm^2
$\sum l_{eff,2}$ =	1050	mm	d_b =	36	mm
t_f =	14	mm	A_s =	1017.36	mm^2
f_y =	420	N/mm^2	bolts no.=	4	
m =	43.75	mm	γ_{M2} =	1	
e_1 = n =	75	mm	k_2 =	0.9	
γ_{M0} =	1				
$M_{pl1,Rd}$ =	21.61	kNm	$F_{t,Rd}$ =	732.4992	kN
$M_{pl2,Rd}$ =	21.61	kNm	$\sum F_{t,Rd}$ =	2929.9968	kN
$F_{T,1,Rd}$ =	1975.68	kN			
$F_{T,2,Rd}$ =	2214.47	kN			
$F_{T,3,Rd}$ =	2930.00	kN			
$F_{T,Rd}$ =	1975.68	kN	β =	$F_{T,1,Rd} / F_{T,2,Rd}$ =	0.89

Table 5.4: Strength of column flange in bending - model 3.

$\sum l_{eff,1}$ =	1050	mm	f_{ub} =	600	N/mm^2
$\sum l_{eff,2}$ =	1050	mm	d_b =	36	mm
t_f =	14	mm	A_s =	1017.36	mm^2
f_y =	420	N/mm^2	bolts no.=	4	
m =	43.75	mm	γ_{M2} =	1	
e_1 = n =	75	mm	k_2 =	0.9	
γ_{M0} =	1				
$M_{pl1,Rd}$ =	21.61	kNm	$F_{t,Rd}$ =	549.3744	kN
$M_{pl2,Rd}$ =	21.61	kNm	$\sum F_{t,Rd}$ =	2197.4976	kN
$F_{T,1,Rd}$ =	1975.68	kN			
$F_{T,2,Rd}$ =	1751.83	kN			
$F_{T,3,Rd}$ =	2197.50	kN			
$F_{T,Rd}$ =	1751.83	kN	β =	$F_{T,1,Rd} / F_{T,2,Rd}$ =	1.13

Table 5.5: Strength of column flange in bending - model 4.

$\sum l_{eff,1}$ =	1050	mm	f_{ub} =	800	N/mm^2
$\sum l_{eff,2}$ =	1050	mm	d_b =	30	mm
t_f =	14	mm	A_s =	706.5	mm^2
f_y =	420	N/mm^2	bolts no.=	4	
m =	43.75	mm	γ_{M2} =	1	
e_1 = n =	75	mm	k_2 =	0.9	
γ_{M0} =	1				
$M_{pl1,Rd}$ =	21.61	kNm	$F_{t,Rd}$ =	508.68	kN
$M_{pl2,Rd}$ =	21.61	kNm	$\sum F_{t,Rd}$ =	2034.72	kN
$F_{T,1,Rd}$ =	1975.68	kN			
$F_{T,2,Rd}$ =	1649.03	kN			
$F_{T,3,Rd}$ =	2034.72	kN			
$F_{T,Rd}$ =	1649.03	kN	β =	$F_{T,1,Rd} / F_{T,2,Rd}$ =	1.20

As already pointed out, to minimize the interaction between the failures modes of the column flange in bending and the failure of the remainder components, the remainder components were made stronger than the column flange in bending. In particular, the beam end plate was defined thick enough to guarantee that the lower collapse mode according to the T-stub model is the mode 3. Table 5.6 presents the computation of the effective length for the beam end plate and Tables 5.7, 5.8, 5.9 and 5.10 represent the strength of the three collapse models of the corresponding T-stub model showing that, for each model, the strength of collapse mode 1 and 2 in the beam end plate is always greater than the strength of mode 3 and is always greater than the strength of the weakest collapse modes of the column flange in bending.

Table 5.6: Effective length for end plate in a bolted connection

Bolt-row location	Bolt row considered individually	
	Circular patterns $l_{eff,\,cp}$ (mm)	Non circular patterns $l_{eff,\,nc}$ (mm)
Bolt row outside tension flange of beam	Smallest of: $2\pi m_x$ $\pi m_x + w$ $\pi m_x + 2e$	Smallest of: $4m_x + 1.25e_x$ $e + 2m_x + 0.625e_x$ $0.5b_p$ $0.5w + 2m_x + 0.625e_x$
	285.77	150
For Mode 1:	$l_{eff,\,1} = l_{eff,\,nc}$ but $l_{eff,\,1} \leq l_{eff,\,cp}$	150
For Mode 2:	$l_{eff,\,2} = l_{eff,\,nc}$	150
m_x = 46.4 mm	w = 150 mm	e_x = 70 mm b_p = 300 mm

Table 5.7: Strength of beam end plate - model 1.

$\sum l_{eff,\,1}$ =	600	mm	f_{ub} =	1000	N/mm^2
$\sum l_{eff,\,2}$ =	600	mm	d_b =	36	mm
t_f =	55	mm	A_s =	1017.36	mm^2
f_f =	420	N/mm^2	bolts no.=	4	
m =	46.4	mm	$\gamma_{M\,2}$ =	1	
$e_x = n$ =	70	mm	k_2 =	0.9	
$\gamma_{M\,0}$ =	1				
$M_{pl\,1,\,Rd}$ =	190.58	kNm	$F_{t,\,Rd}$ =	915.624	kN
$M_{pl\,2,\,Rd}$ =	190.58	kNm	$\sum F_{t,\,Rd}$ =	3662.496	kN
$F_{T,1,\,Rd}$ =	16428.88	kN			
$F_{T,\,2,\,Rd}$ =	5477.02	kN			
$F_{T,3,\,Rd}$ =	3662.50	kN			
$F_{T,\,Rd}$ =	3662.50	kN			

Table 5.8: Strength of beam end plate - model 2.

$\sum l_{eff,\,1}$ =	600	mm	f_{ub} =	800	N/mm^2
$\sum l_{eff,\,2}$ =	600	mm	d_b =	36	mm
t_f =	55	mm	A_s =	1017.36	mm^2
f_f =	420	N/mm^2	bolts no.=	4	
m =	46.4	mm	$\gamma_{M\,2}$ =	1	
$e_x = n$ =	70	mm	k_2 =	0.9	
$\gamma_{M\,0}$ =	1				
$M_{pl\,1,\,Rd}$ =	190.58	kNm	$F_{t,\,Rd}$ =	732.4992	kN
$M_{pl\,2,\,Rd}$ =	190.58	kNm	$\sum F_{t,\,Rd}$ =	2929.9968	kN
$F_{T,1,\,Rd}$ =	16428.88	kN			
$F_{T,\,2,\,Rd}$ =	5036.51	kN			
$F_{T,3,\,Rd}$ =	2930.00	kN			
$F_{T,\,Rd}$ =	2930.00	kN			

Table 5.9: Strength of beam end plate - model 3.

$\sum l_{eff,\,1}$ =	600	mm	f_{ub} =	600	N/mm^2
$\sum l_{eff,\,2}$ =	600	mm	d_b =	36	mm
t_f =	55	mm	A_s =	1017.36	mm^2
f_f =	420	N/mm^2	bolts no.=	4	
m =	46.4	mm	$\gamma_{M\,2}$ =	1	
e_x = n =	70	mm	k_2 =	0.9	
$\gamma_{M\,0}$ =	1				
$M_{pl\,1,\,Rd}$ =	190.58	kNm	$F_{t,\,Rd}$ =	549.3744	kN
$M_{pl\,2,\,Rd}$ =	190.58	kNm	$\sum F_{t,\,Rd}$ =	2197.4976	kN
$F_{T,1,\,Rd}$ =	16428.88	kN			
$F_{T,\,2,\,Rd}$ =	4596.00	kN			
$F_{T,3,\,Rd}$ =	2197.50	kN			
$F_{T,\,Rd}$ =	2197.50	kN			

Table 5.10: Strength of beam end plate - model 4.

$\sum l_{eff,\,1}$ =	600	mm	f_{ub} =	1000	N/mm^2
$\sum l_{eff,\,2}$ =	600	mm	d_b =	30	mm
t_f =	55	mm	A_s =	706.5	mm^2
f_f =	420	N/mm^2	bolts no.=	4	
m =	46.4	mm	$\gamma_{M\,2}$ =	1	
e_x = n =	70	mm	k_2 =	0.9	
$\gamma_{M\,0}$ =	1				
$M_{pl\,1,\,Rd}$ =	190.58	kNm	$F_{t,\,Rd}$ =	635.85	kN
$M_{pl\,2,\,Rd}$ =	190.58	kNm	$\sum F_{t,\,Rd}$ =	2543.4	kN
$F_{T,1,\,Rd}$ =	16428.88	kN			
$F_{T,\,2,\,Rd}$ =	4804.02	kN			
$F_{T,3,\,Rd}$ =	2543.40	kN			
$F_{T,\,Rd}$ =	2543.40	kN			

5.2. Monotonic Behaviour

For monotonically loaded models, an imposed displacement was applied in the boundary conditions as described in previous chapter, the solution was obtained in 3 steps.

First step was used to formulate the boundary conditions and interactions, as explained in the previous chapters. The second step was used to for the pre-loading of the bolts, using the adjust length option and calculation the length magnitude by the elastic elongation needed to simulate the required amount of force in the bolts, 80 % of the bolt yield axial force was used. Finally, in third step, a pushover analysis was performed.

5.2.3. Column Flange in Bending

The main objective of monotonic analysis was to compare the strength of the column flange in bending of the FEM with strength to be expected according to the T-stub model from EC3-1-8 and presented in section 5.2.1.

During the course this work was not possible to reach the collapse of the FEM models due to convergence issues. Accordingly, the strength computed according to EC3-1-8 was compared with the internal force corresponding to the end of the elastic regime in the FEM models.

To identify the response of column flange models from numerical analysis, applied monotonic loads were gathered from the FEM model and deformation (δ) of T-stub models were computed by subtracting the deformation (U) at column´s web from the average deformation (U_1+U_2)/2 at bolt holes, shown in Figure 5.1 has suggested by Hugo [11].

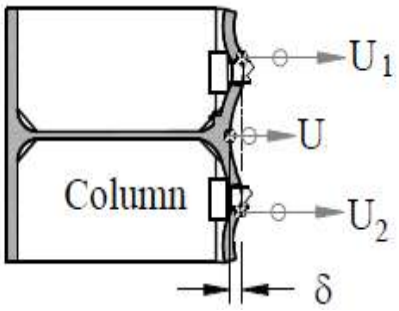

Figure 5.1: Predefine nodes to assess the deformation of column flange in bending [11]

The force corresponding to the elastic regime was assumed to correspond to the point of intersection of the two straight lines arising from bilinear approximation [17] of the force displacement curves, shown in Figure 5.2, Figure 5.3, Figure 5.4, and Figure 5.5 - the bilinear approximation was derived through regression analysis. For regression analysis, two lines were drawn, blue and orange lines, on a Force-Deformation curved of models, taking into account that blue line should characterize the part of the load-deformation curve before the yielding (approximately 55% of maximum load, obtained through F-δ curve) and the orange line should characterize the part of the curve after the yielding.

Figure 5.6 compares the monotonic behaviour of the column flange in bending from all the models and Table 5.11 shows the comparison of the elastic limit computed as mentioned in the formed paragraph with the strength of the column flange in bending computed using the T-Stub model for EC3-1-8.

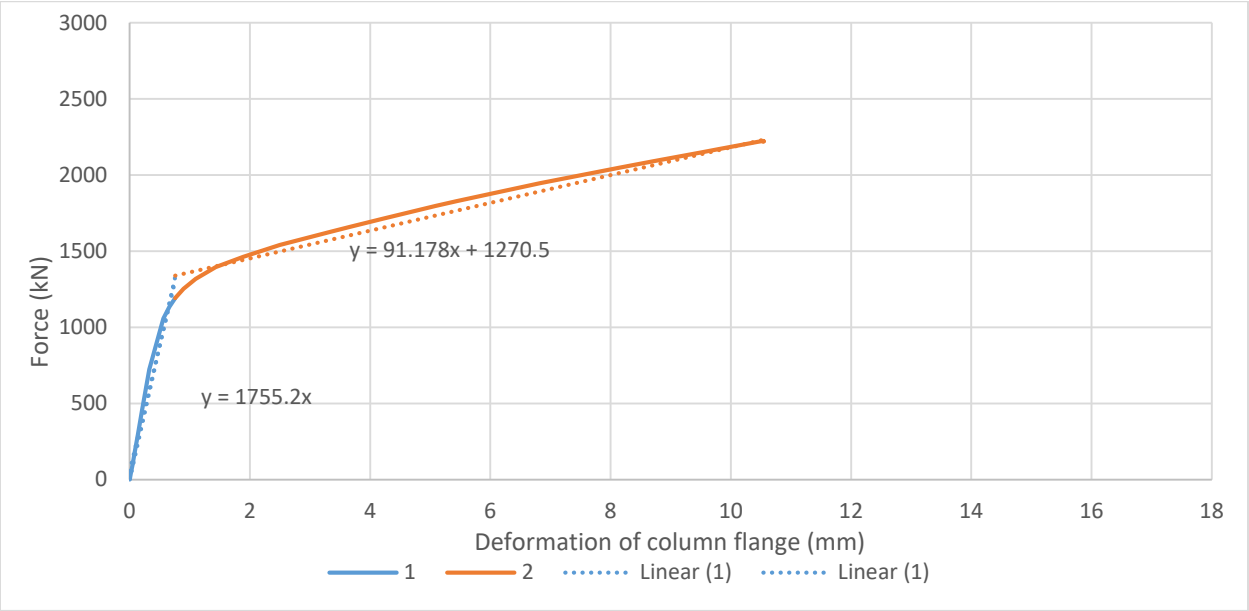

Figure 5.2: Force-Deformation curve and bilinear approximation for the column flange in bending in model 1

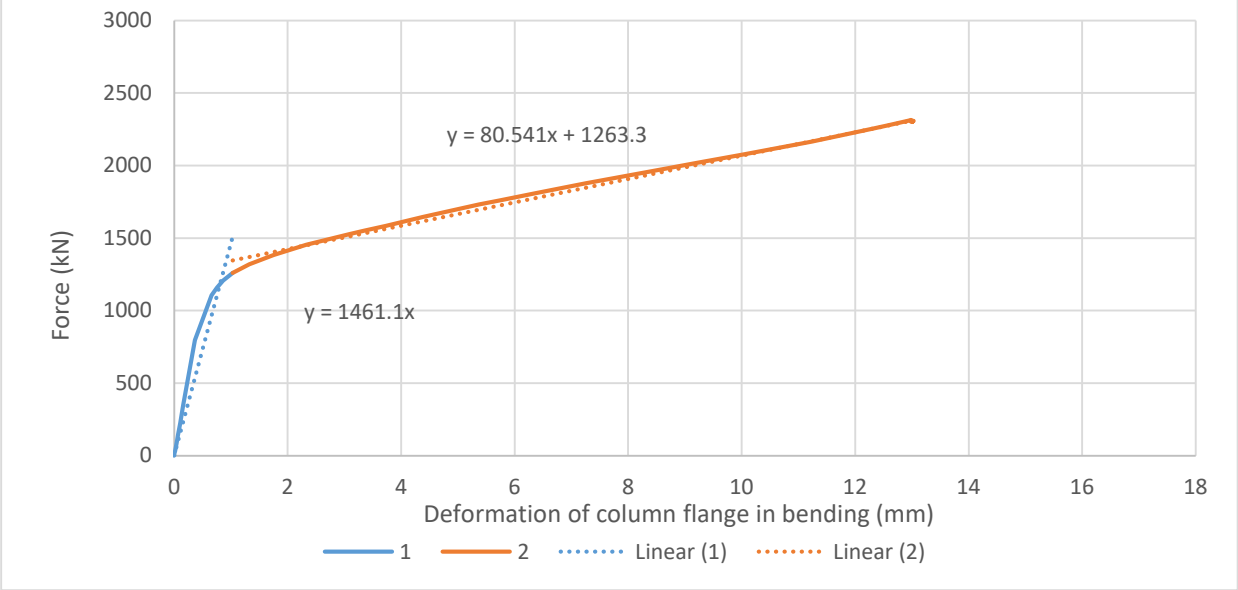

Figure 5.3: Force-Deformation curve and bilinear approximation for the column flange in bending in model 2

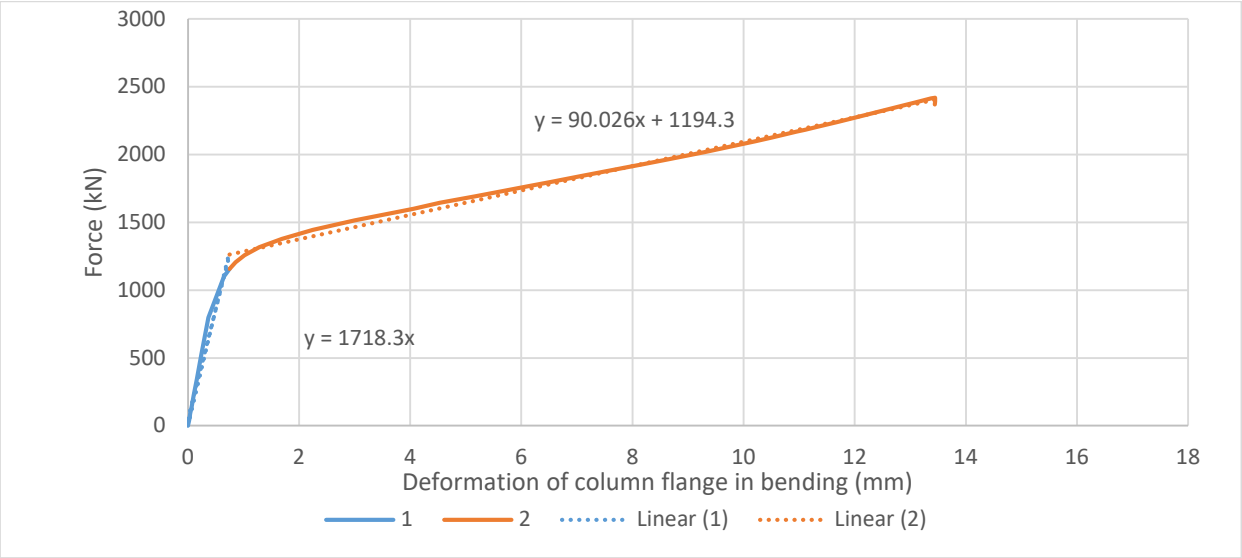

Figure 5.4: Force-Deformation curve and bilinear approximation for the column flange in bending in model 3

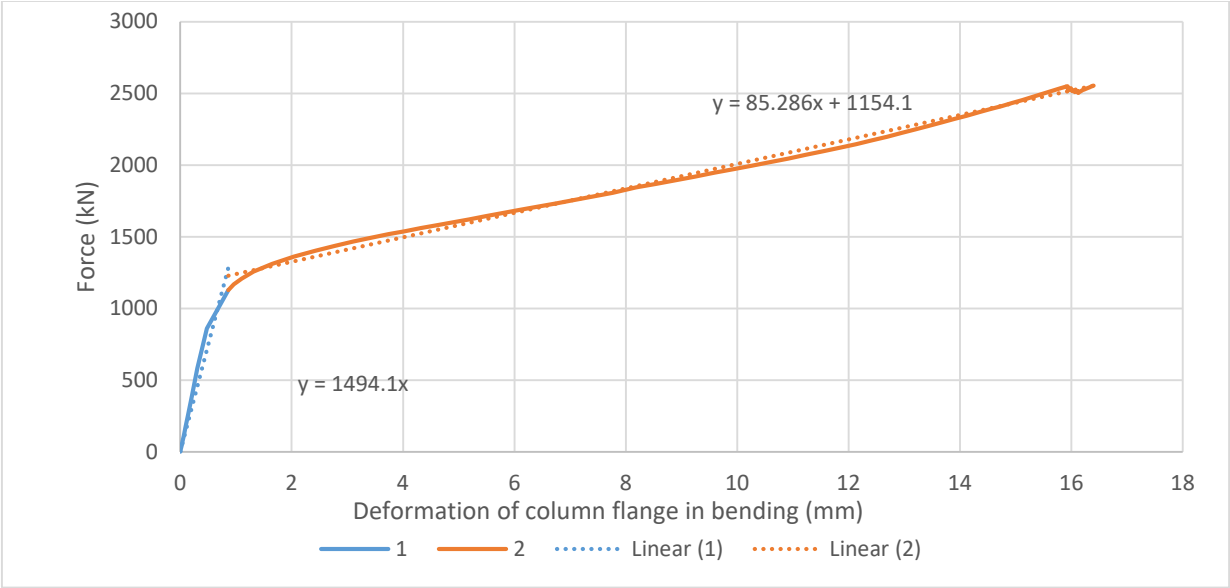

Figure 5.5: Force-Deformation curve and bilinear approximation for the column flange in bending in model 4

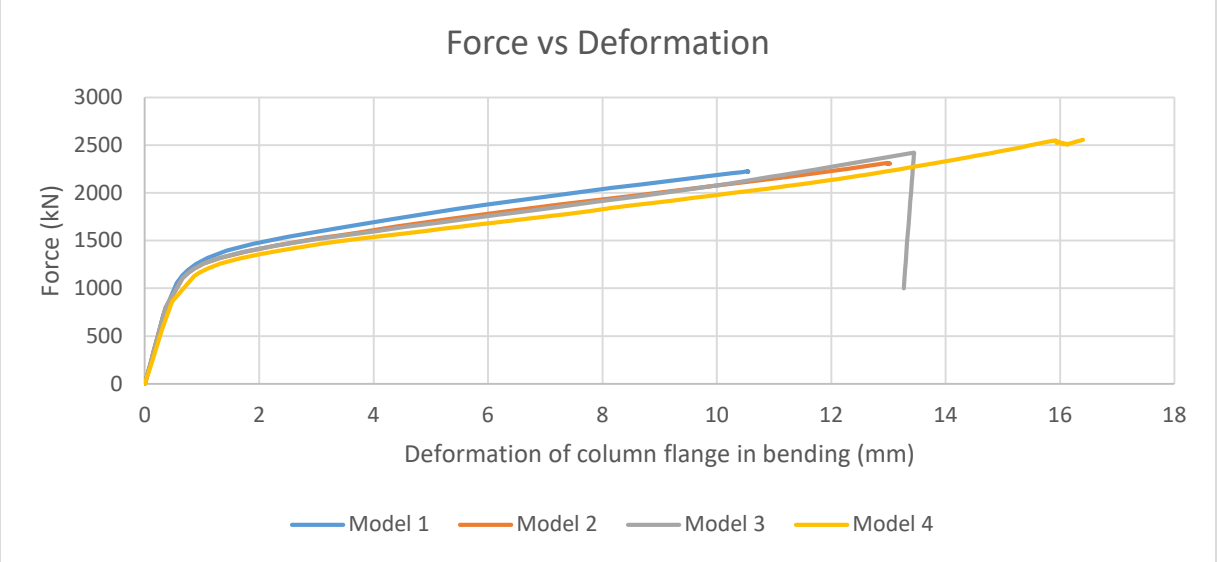

Figure 5.6: Force-Deformation curves for the column flange in bending

Table 5.11: Comparison of T-stub response obtained from EC3-1-3 and numerical models

Model	Bolt	Failure Mode	EC3-1-8		Analytical Results	Deviation
			$F_{t,Rd}$ (kN)	β	$F_{t,Rd}$ (kN)	%
1	M36 (10.9)	Mode 1	1975.68	0.74	1341.12	32.17
2	M36 (8.8)	Mode 1	1975.68	0.89	1337.00	32.33
3	M36 (6.8)	Mode 2	1751.83	1.13	1260.51	28.05
4	M30 (10.9)	Mode 2	1649.03	1.2	1223	25.78

Having into account that the T-Stub models considered in EC3-1-8 rely in the formation of a plastic mechanism to compute their strength it is expected that the strength computed using these simplified T-Stub models to be higher than the force corresponding to the end of the elastic regime computed as explained previously and shown in Figure 5.2, Figure 5.3, Figure 5.4, and Figure 5.5. The results in Table 5.11 confirm these expectation showing that the strength computed from the T-Stub models is 25 to 35% higher than the force corresponding to the end of the elastic regime of the column flange in bending in the FEM models.

Figure 5.6 shows that the smaller the β, the stiffer the column flange in bending, however the differences between the four models are small. To assess the influence of the β parameter in the shape of the force-deformation relation of the column flange in bending the curves shown in Figure 5.6 was normalizing by getting the maximum forces of each curves in the range [0, 10] mm and dividing the forces in that range by that force, see Figure 5.7. It reveals that no huge variances are to be predicted from the normalized curves.

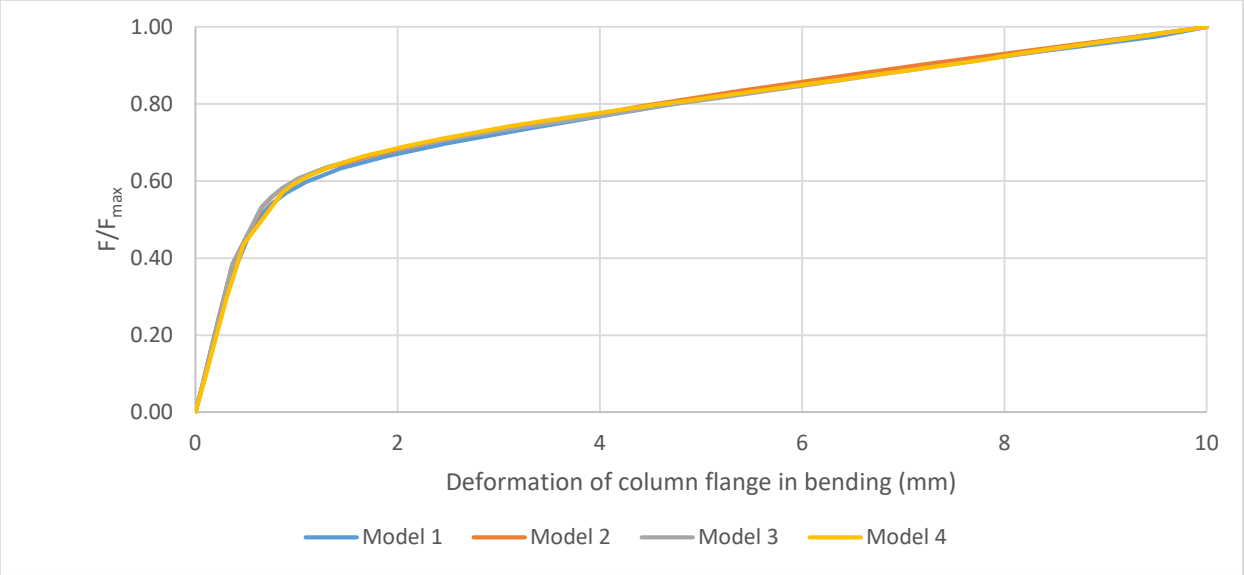

Figure 5.7: Normalized Force-Deformation curves for monotonically loaded models

5.2.4. Overall Model

Figure 5.8 shows the force-deformation relations for the FEM models where the forces and deformations were both gathered from RP3 in the FEM models. These curves characterize the behaviour of the entire tension region of the beam-to-column joint. i.e. the beam flange in tension, the end plate in bending, the bolts in tension, the column flange in bending and the column web in tension (with the stiffener) – actually the column in bending is also considered. Figure 5.8 shows that the smaller the β the stiffer the tension region, however the differences between the four models are small.

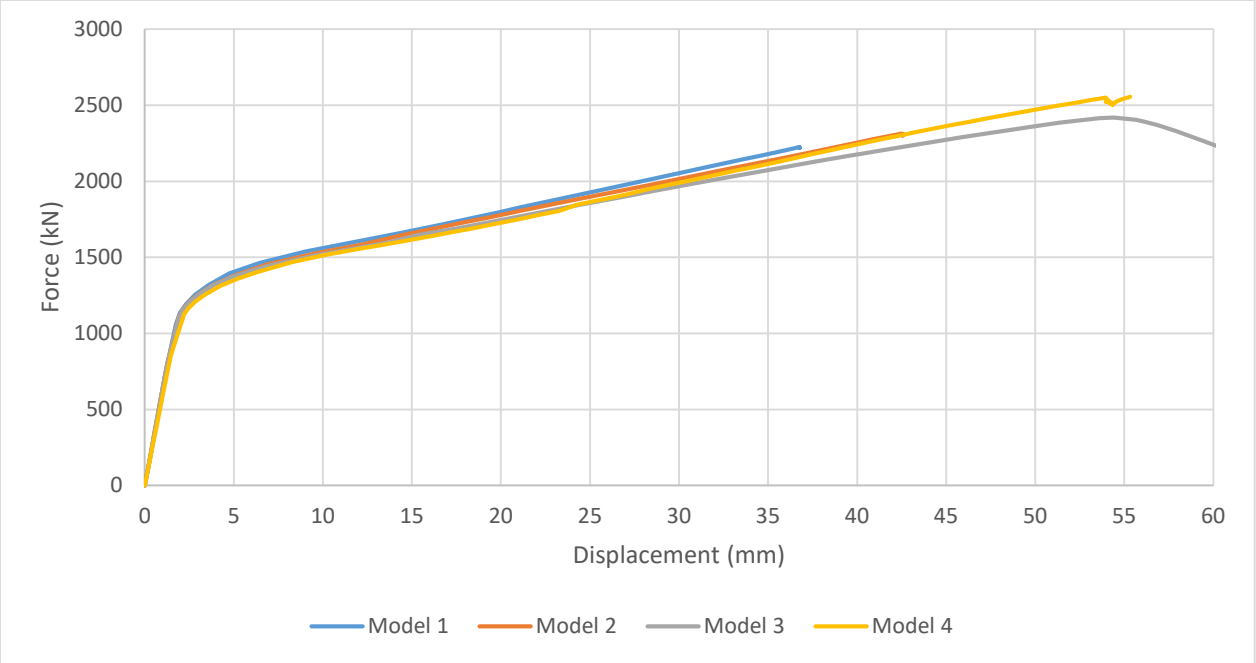

Figure 5.8: Force-Displacement curves for monotonically loaded model of joints

Figure 5.9 shows the normalized force vs. displacement relation for the four models – the normalization was performed using the same procedure used for the force vs deformations of the column flange in bending. It demonstrates that there is no large difference after normalization of F-δ curve.

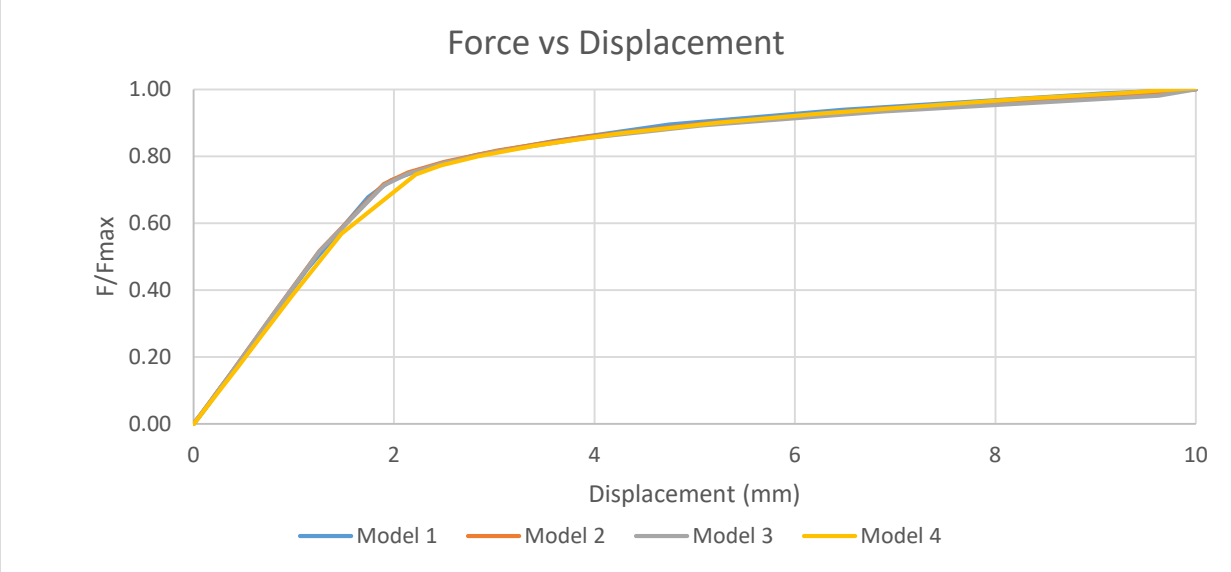

Figure 5.9: Normalized Force-Displacement curves for monotonically loaded model of joints

In Figure 5.10, the Von Mises stresses are drawn, emphasizing the formulation of failure modes, as predicted the complete yielding of column flange or partial yielding of column flange for failure mode 1 or failure mode 2 respectively. In Figure 5.10, on left hand sides, whole model is shown while on right hand side, column flange strength is shown.

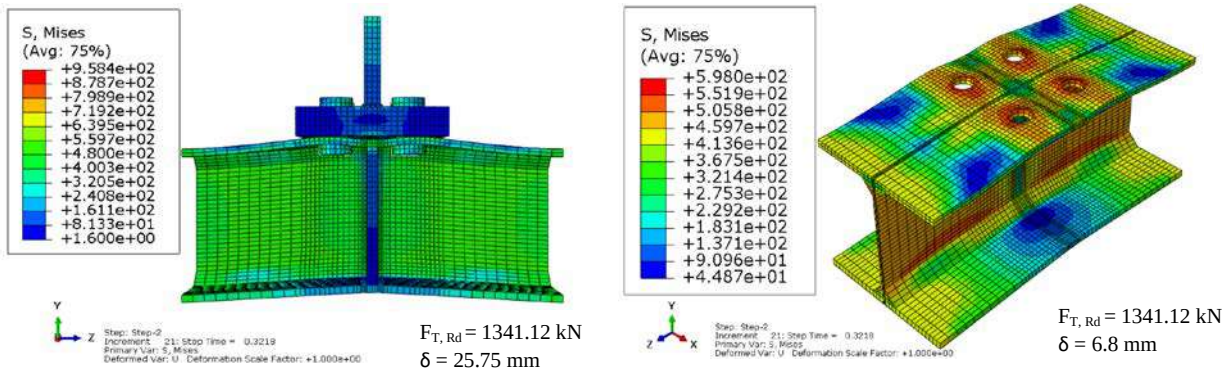

$F_{T, Rd}$ = 1341.12 kN
δ = 25.75 mm

$F_{T, Rd}$ = 1341.12 kN
δ = 6.8 mm

Model 1

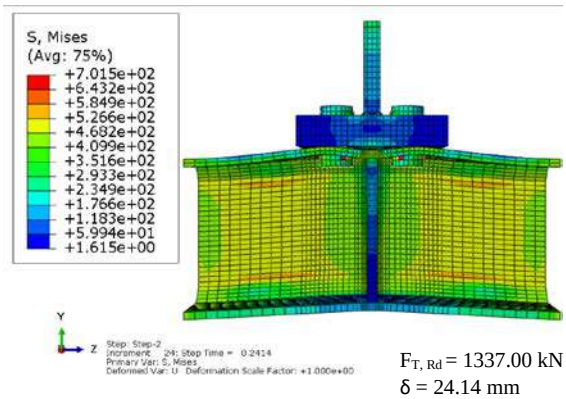

$F_{T, Rd}$ = 1337.00 kN
δ = 24.14 mm

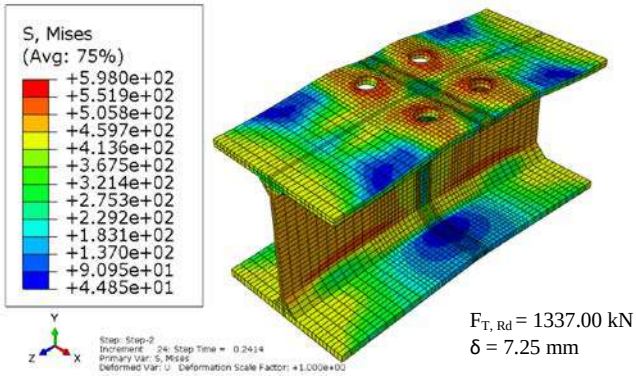

$F_{T, Rd}$ = 1337.00 kN
δ = 7.25 mm

Model 2

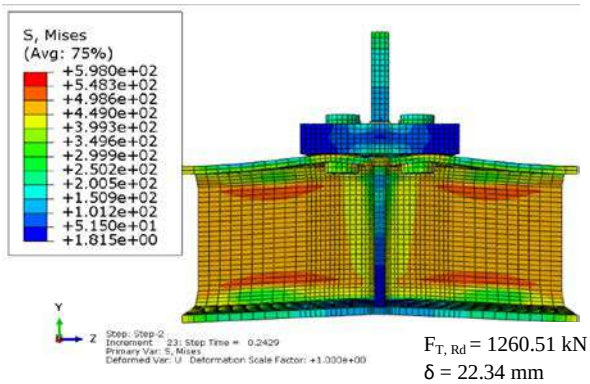

$F_{T, Rd}$ = 1260.51 kN
δ = 22.34 mm

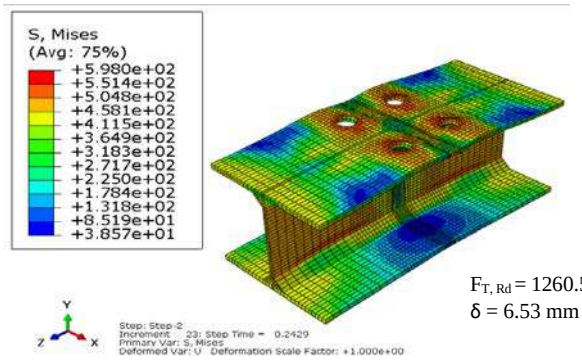

$F_{T, Rd}$ = 1260.51 kN
δ = 6.53 mm

Model 3

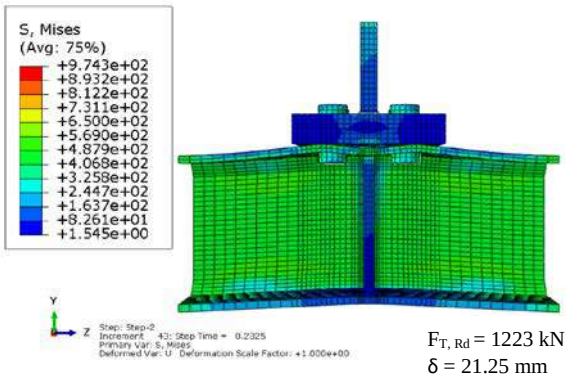

$F_{T, Rd}$ = 1223 kN
δ = 21.25 mm

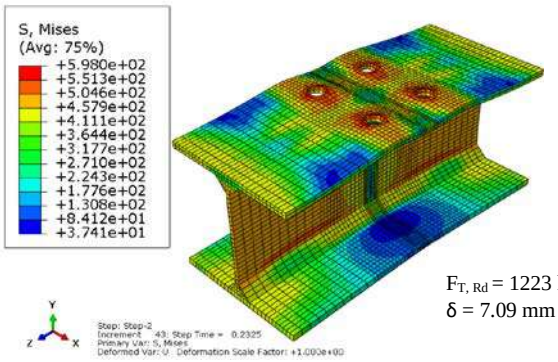

$F_{T, Rd}$ = 1223 kN
δ = 7.09 mm

Model 4

Figure 5.10:Von Mises stress for monotonically loaded models

5.3. Cyclic Behaviour

The cyclic analysis of the FEM models followed the same procedure as described for monotonically loaded models. The load history was applied imposing the load protocol described in section 4.2 to the RP3.

Again, due to convergence issues, in the course of the present work it was not possible to reach the collapse of the models. This way, the cyclic behavior of the models was studied only for the first 24 cycles of the loading protocol defined in section 3.5.

5.3.1. Column Flange in Bending

Figure 5.11, Figure 5.12, Figure 5.13, and Figure 5.14 show the cyclic and the monotonic force vs. deformation of the column flange in bending of the four models described in section 5.1.

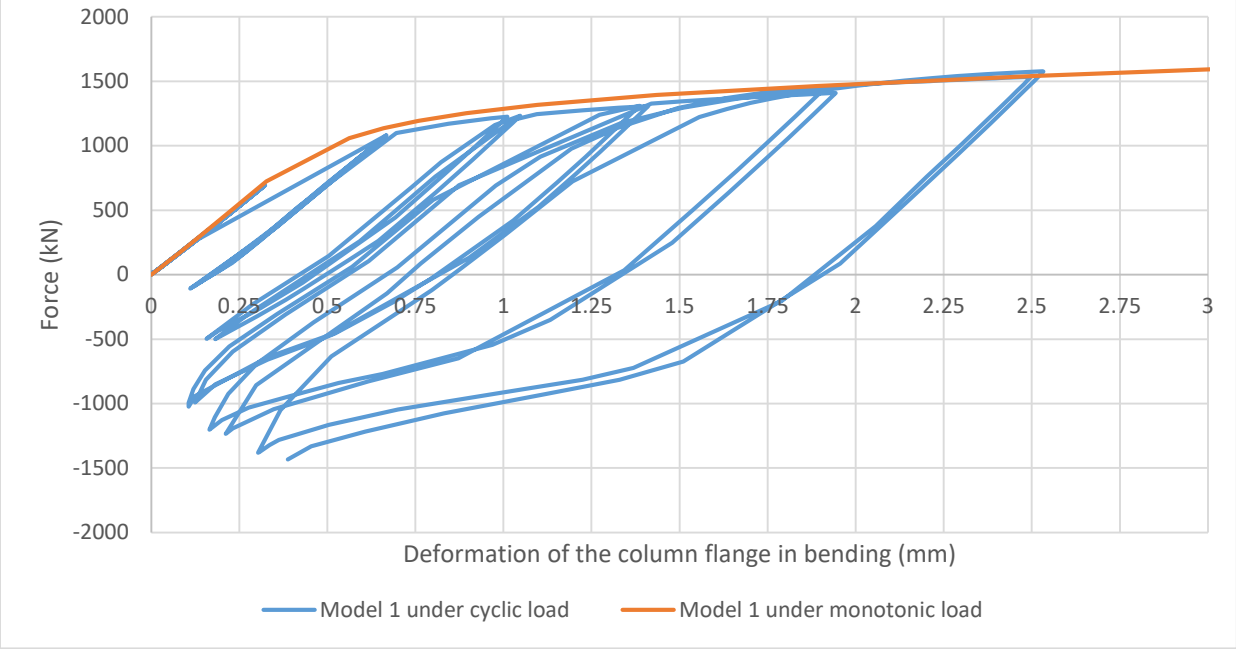

Figure 5.11: Force-Deformation curves for the column flange in bending under cyclic and monotonic loads – model 1.

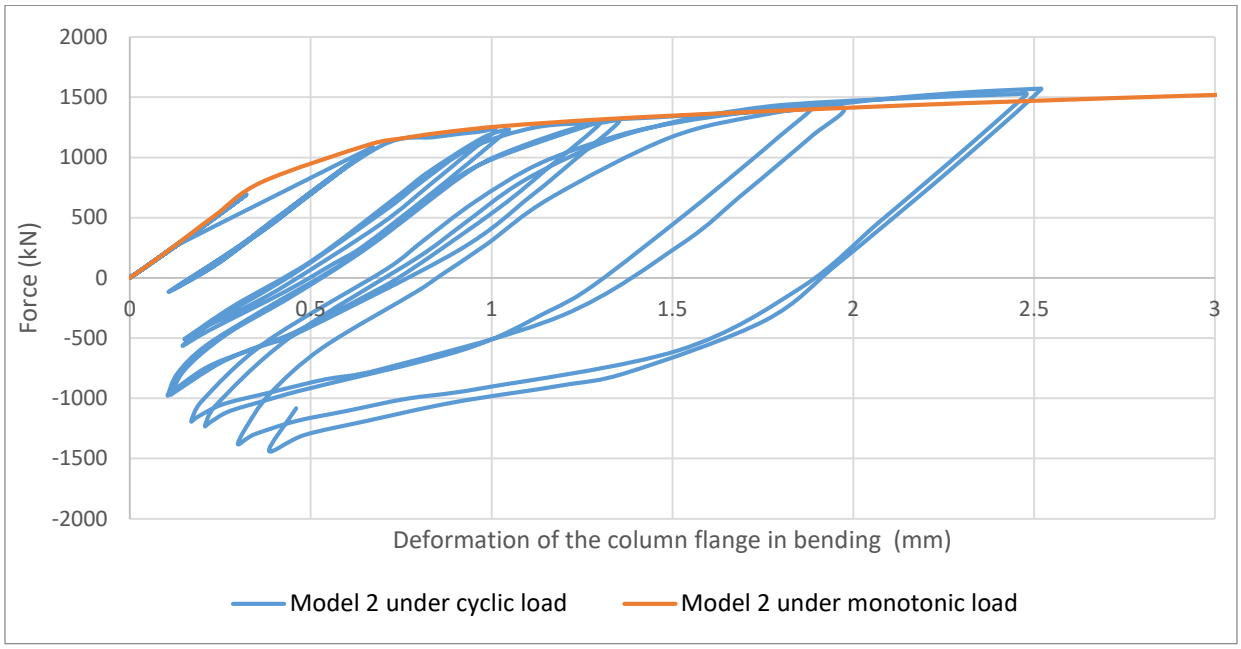

Figure 5.12: Force-Deformation curves for the column flange of Model 2 under cyclic and monotonic loads

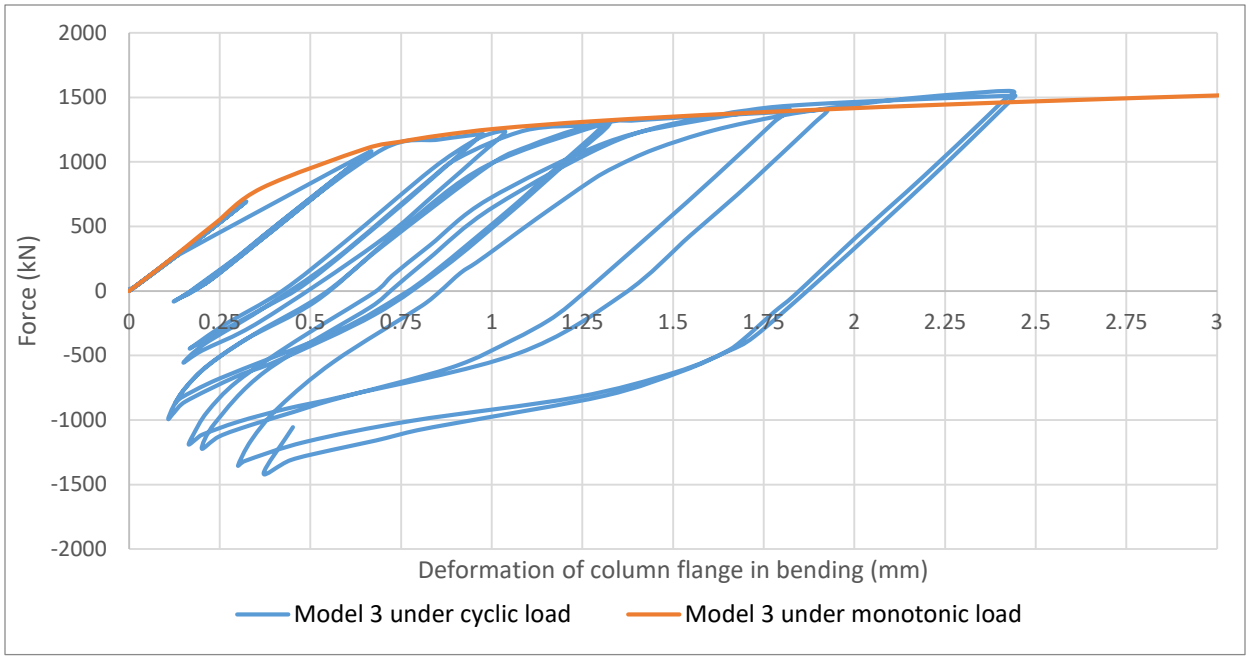

Figure 5.13: Force-Deformation curves for the column flange of Model 3 under cyclic and monotonic loads

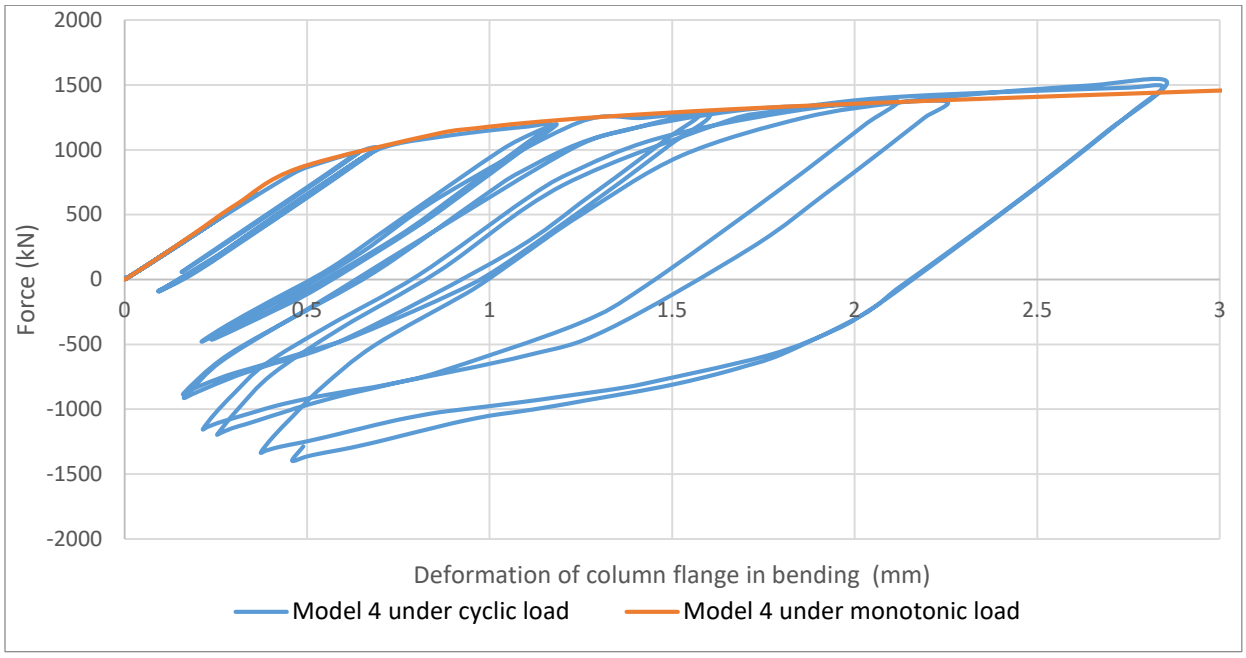

Figure 5.14: Force-Deformation curves for the column flange of Model 4 under cyclic and monotonic loads

Figure 5.11, Figure 5.12, Figure 5.13, and Figure 5.14 show that, irrespective of the value of β in the first 24 cycles in the four models:

(i) No strength degradation is found – there is a good agreement between the monotonic force-deformation curve and the envelope of the cyclic curve

(ii) No stiffness degradation is found – the reloading branch in all the cycles is approximately parallel; actually in some of the models the cyclic curve surpasses the monotonic one showing some hardening;

(iii) No pinching effect is found – the cycles are wide and stable.

Figure 5.15 presents the force vs deformation curves of the column flange in bending of all the four models showing that models 1, 2 and 3 present a response fairly similar but model 4 (the model with highest β) clearly shows bigger deformation in the last cycles.

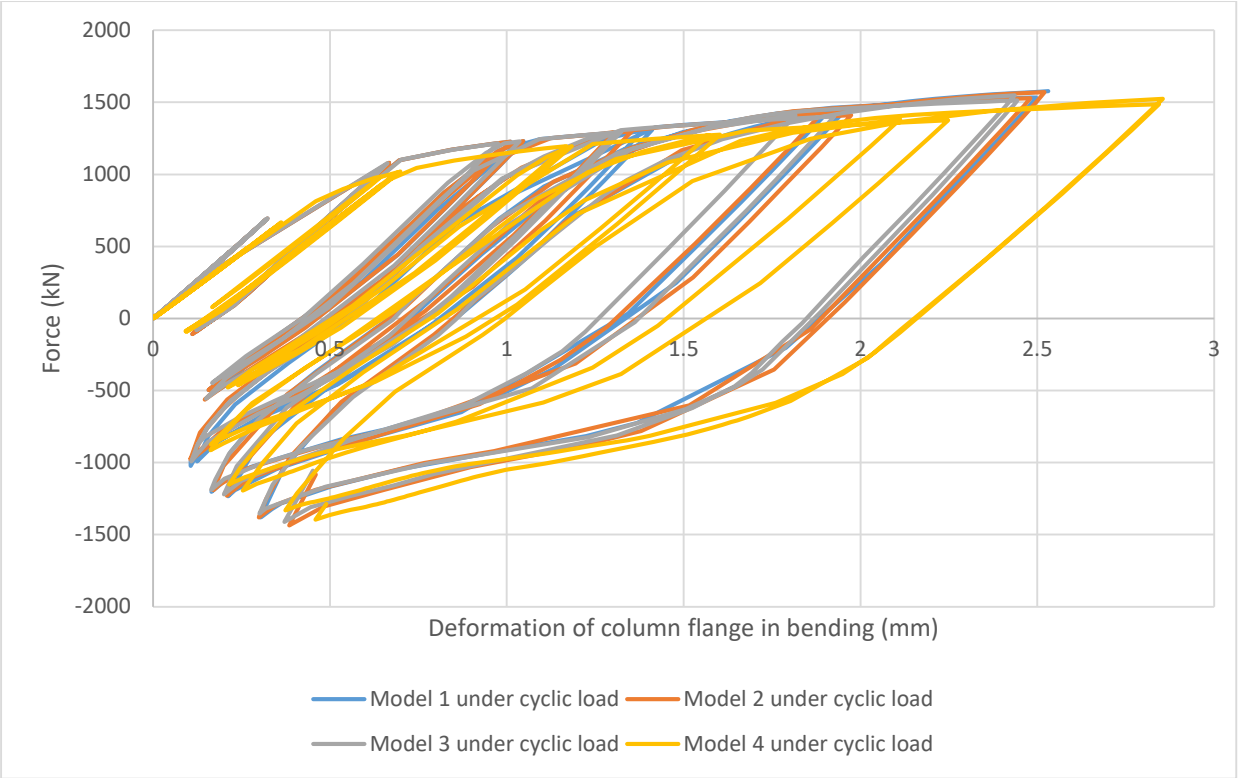

Figure 5.15: Force-Deformation curves for the column flange of All Models under cyclic loads

Figure 5.16 presents the again the cyclic behavior of the column flange in bending for all the four models but the forces were normalized by dividing it by the maximum force attained in the range 3 mm in each model. Figure 5.16 shows the same trends already discussed for Figure 5.15.

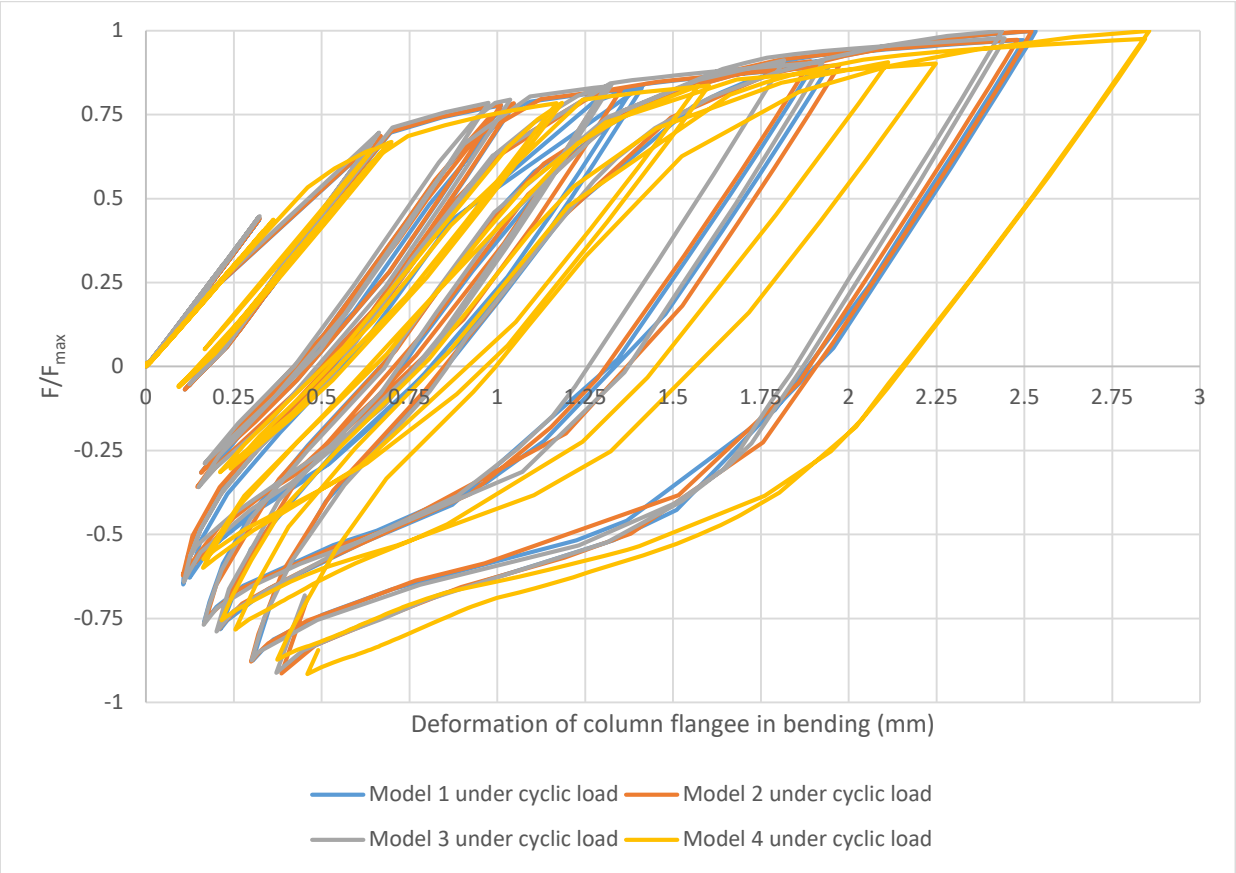

Figure 5.16: Normalized Force-Displacement curves for cyclic loaded models

Table 5.12, Figure 5.17 and Figure 5.18 show the dissipation of energy by column flange in bending for every 6 cyclic interval. As expected the energy dissipation increases with the amplitudes of the cycles. Comparison of energy dissipation between all models, revealed that for first 6 cycles energy dissipation is almost same in all of them except model 4. However, for large amplitude cycles, the energy dissipation in model 4 is clearly higher than in model 1, showing an increases with the increase of the parameter β, however the trend is not clear because model 2 and 3 for cycles 7-12 show lower energy dissipation than model 1. On the other hand, the accumulated energy dissipation of column flange in bending after 24 cycles increases with the increase of the parameter β, with the exception of model 2.

Table 5.12: Energy dissipation for the column flange in bending (J).

No. of Cycles	Model 1		Model 2		Model 3		Model 4	
	In the cycles	Σ	In the cycles	Σ	In the cycles	Σ	In the cycles	Σ
0-6	76.79	76.79	76.79	76.79	76.79	76.79	17.02	17.02
7-12	235.84	312.63	220.80	297.58	198.56	275.35	65.79	82.81
13-18	305.73	618.36	371.44	669.02	301.95	577.30	688.58	771.40
19-24	8939.60	9557.96	9235.12	9904.15	8842.59	9419.89	10332.10	11103.49

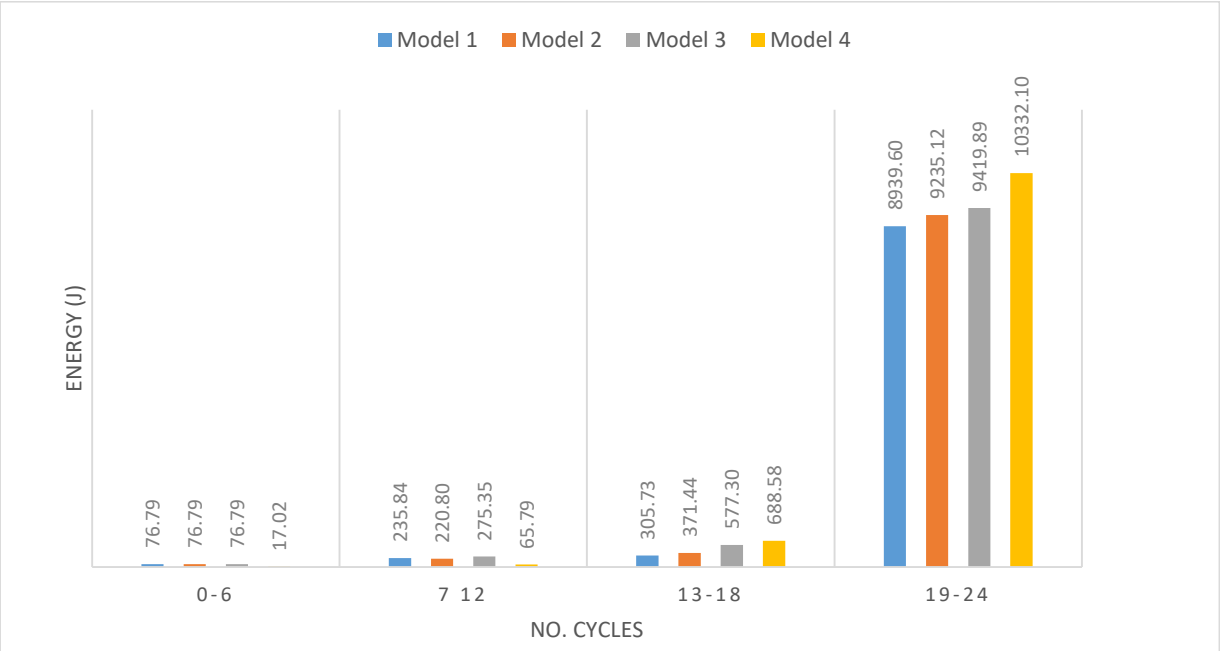

Figure 5.17: Energy dissipation in the column flange in bending.

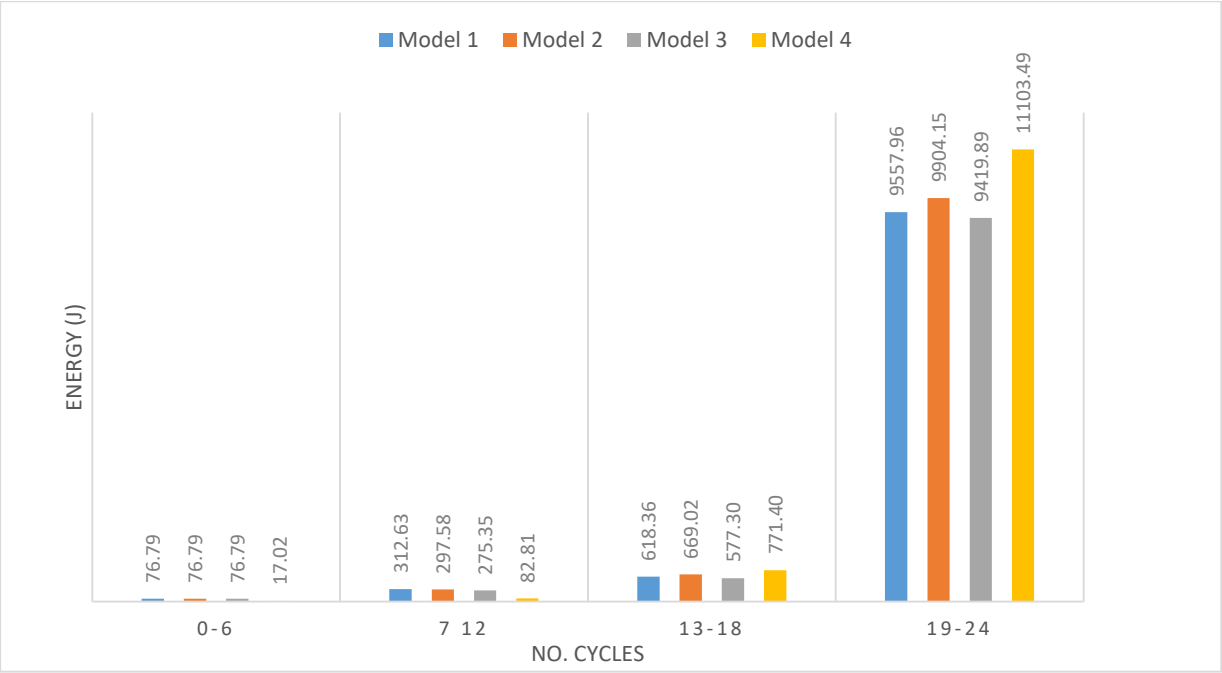

Figure 5.18: Accumulative energy dissipation in the column flange in bending.

Table 5.13, Figure 5.19 and Figure 5.20 present the energy dissipation computed making use of the normalized force vs deformation curves for the column flange in bending to remove the effect of the strength of each model. Roughly, the same conclusion gathered from Table 5.12, Figure 5.17 and Figure 5.18 apply.

Table 5.13: Normalized energy dissipation for the column flange in bending

No. of Cycles	Model 1		Model 2		Model 3		Model 4	
	In the cycles	∑	In the cycles	∑	In the cycles	∑	In the cycles	∑
0-6	0.05	0.05	0.05	0.05	0.05	0.05	0.01	0.01
13-18	0.15	0.20	0.14	0.19	0.13	0.18	0.04	0.05
7 12	0.19	0.39	0.24	0.43	0.20	0.37	0.45	0.51
19-24	5.96	6.35	5.88	6.30	5.71	6.09	6.78	7.29

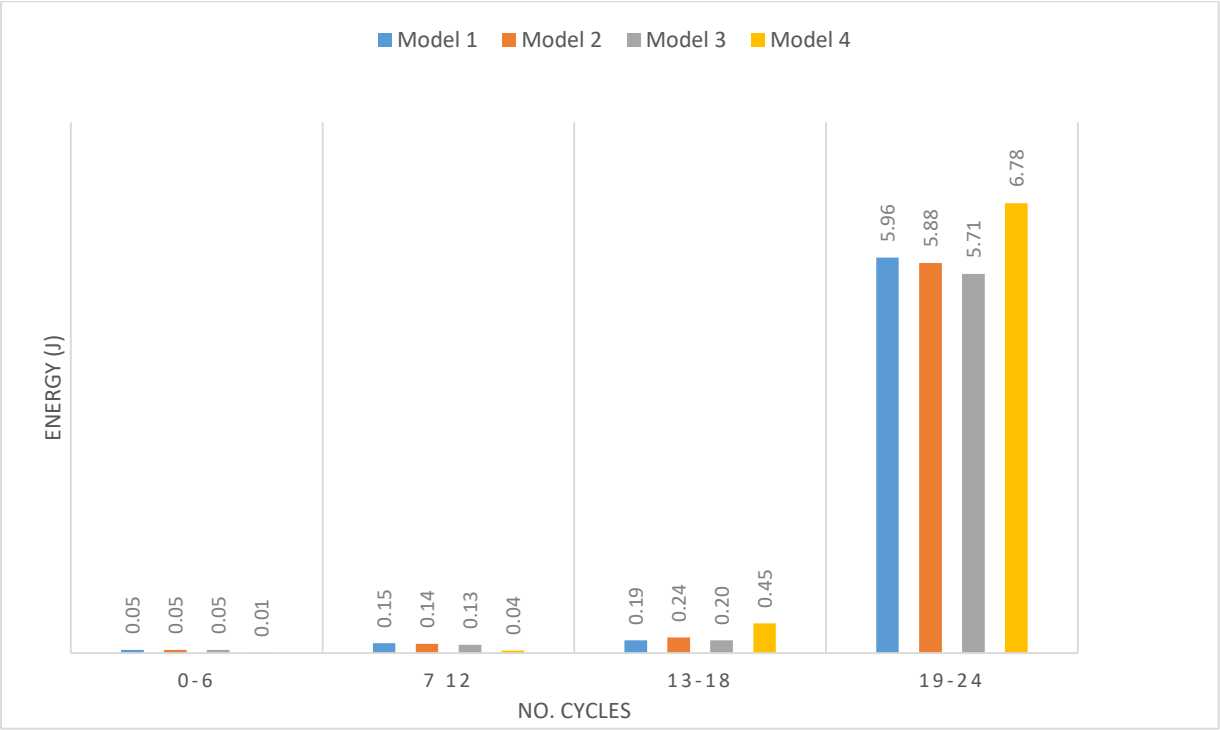

Figure 5.19: Normalized energy dissipation for the column flange in bending

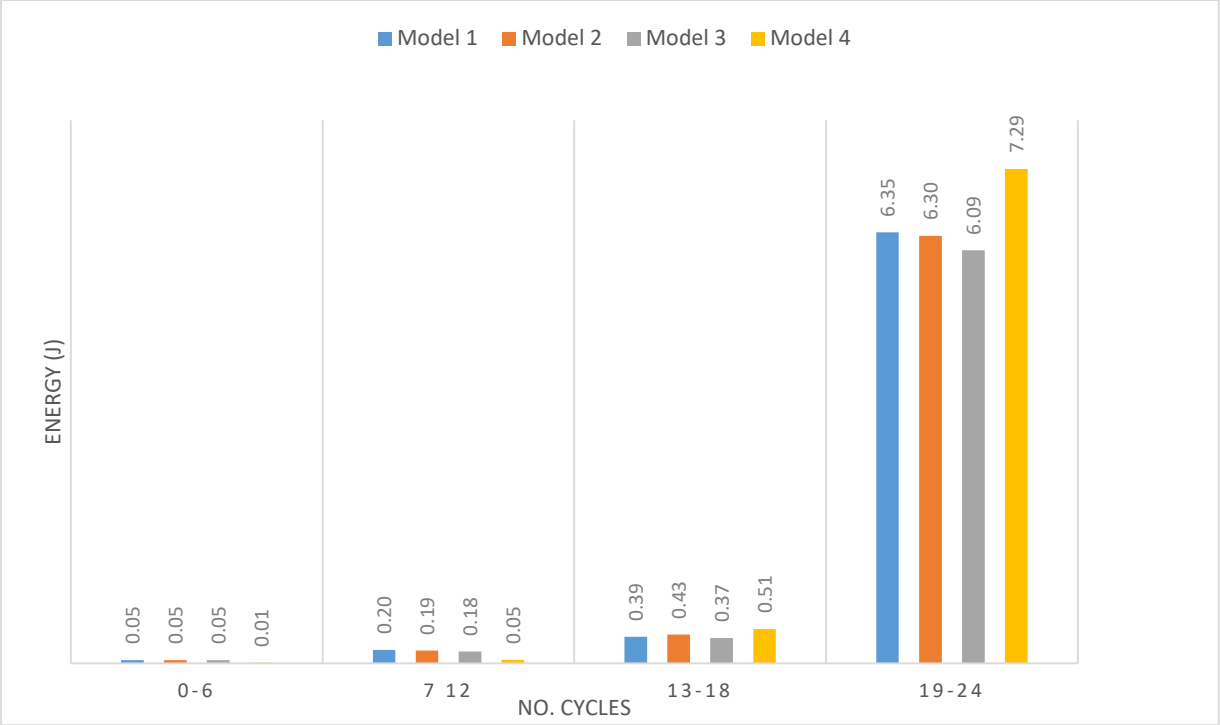

Figure 5.20: Accumulative normalized energy dissipation for the column flange in bending

5.3.2. Overall Model

Figure 5.21 shows the force-deformation relations for the FEM models where the force and deformation were both gathered from RP3 in the FEM models. As already stated, these curves characterize the behaviour of the entire tension region of the beam-to-column joint. i.e. the beam flange in tension, the end plate in bending, the bolts in tension, the column flange in bending and the column web in tension (with the stiffener).

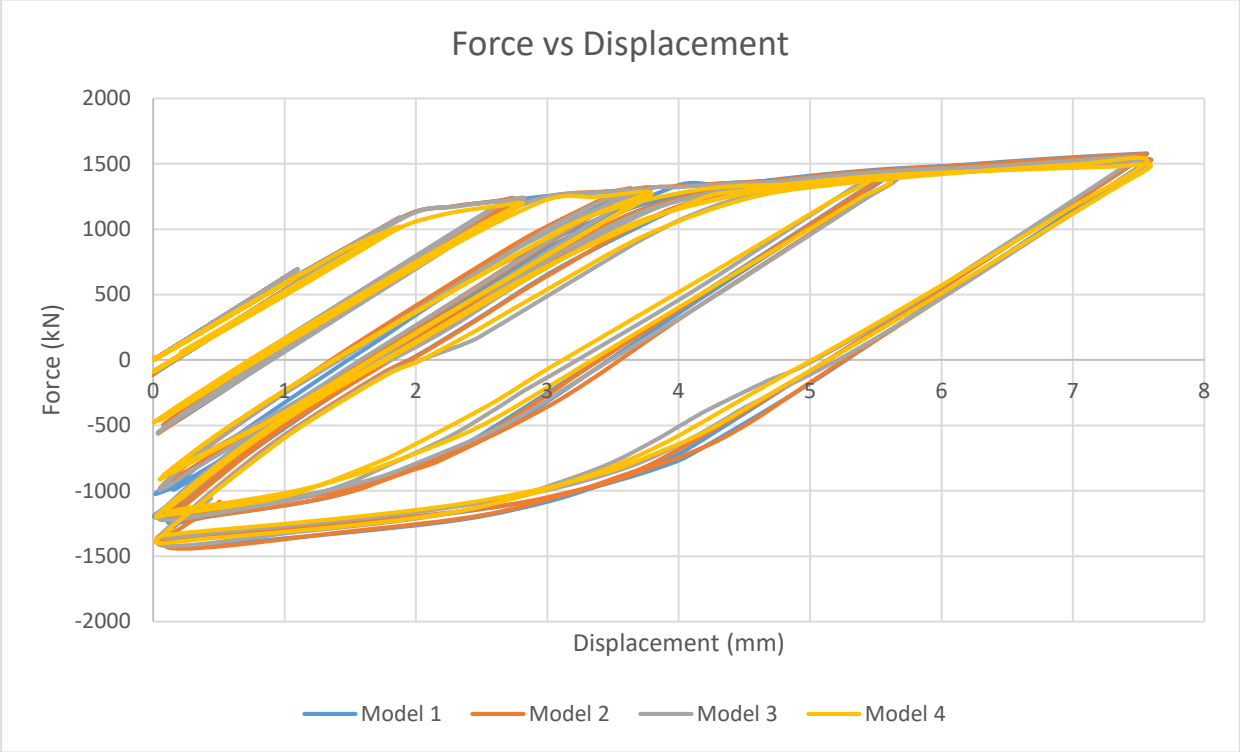

Figure 5.21: Force-Displacement curves for cyclic loaded models

Figure 5.22 represent the normalized form of Force-Displacement curves obtained using a procedure similar to the one used for the force vs deformation curves of the column flange in bending.

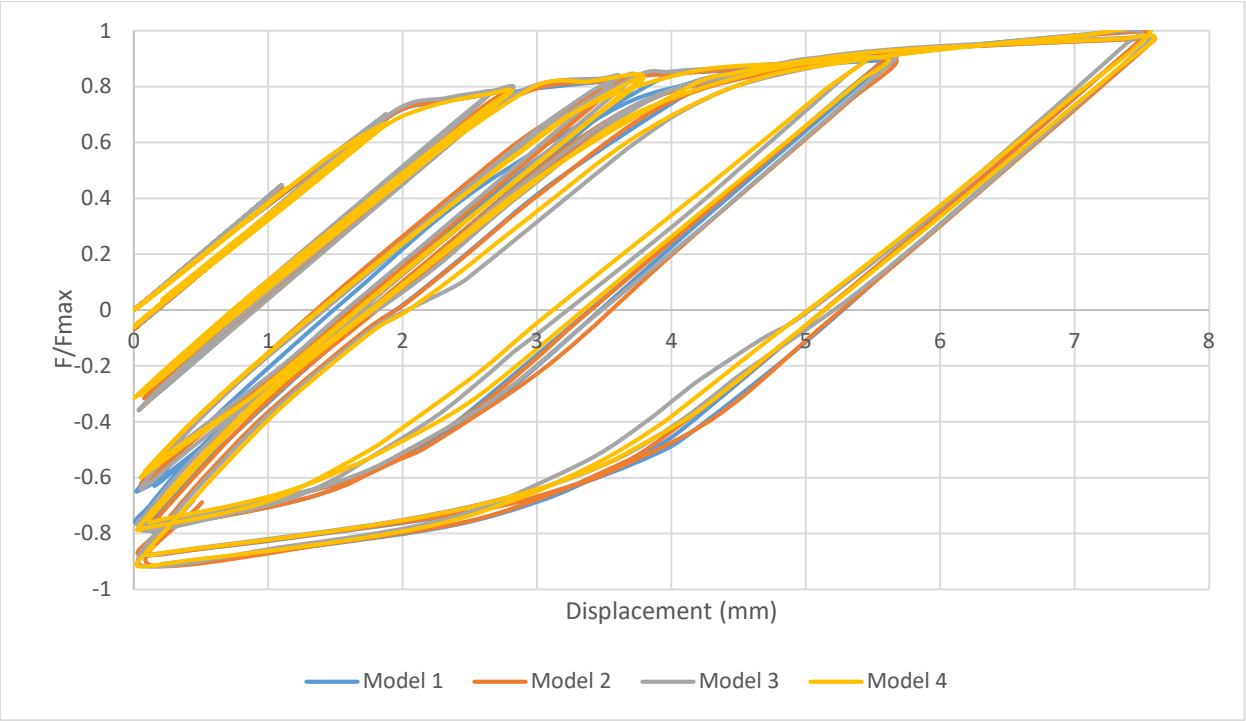

Figure 5.22: Normalized Force-Displacement curves for cyclic loaded models

Both Figure 5.21 and Figure 5.22 show that the parameter β has a smaller influence in the overall behaviour of the tension zone of the beam-to-column joint. This means that, e.g. the larger deformation shown by the column flange in bending in Figure 5.15 are compensated with smaller deformation in other parts of the tension region.

Table 5.14, Figure 5.23 and Figure 5.24 shows energy dissipation by the entire joint models. For first 6 cyclic intervals, dissipation of energy is same in all models except model 4. It is also perceived that β has significant relation with accumulation of energy of entire joint under cyclic loading conditions, β is inversely proportional to energy dissipated by entire joint.

Table 5.14: Energy dissipation for the entire joint model (J).

No. of Cycles	Model 1		Model 2		Model 3		Model 4	
	In the cycles	∑	In the cycles	∑	In the cycles	∑	In the cycles	∑
0-6	261.5	261.5	261.5	261.5	261.5	261.5	57.3	57.3
7-12	380.6	642.1	337.7	599.2	350.7	612.2	207.2	264.5
13-18	764.6	1406.7	989.7	1588.9	763.0	1375.3	913.9	1178.5
19-24	28621.6	30028.3	27914.5	29503.4	25352.7	26727.9	25473.8	26652.3

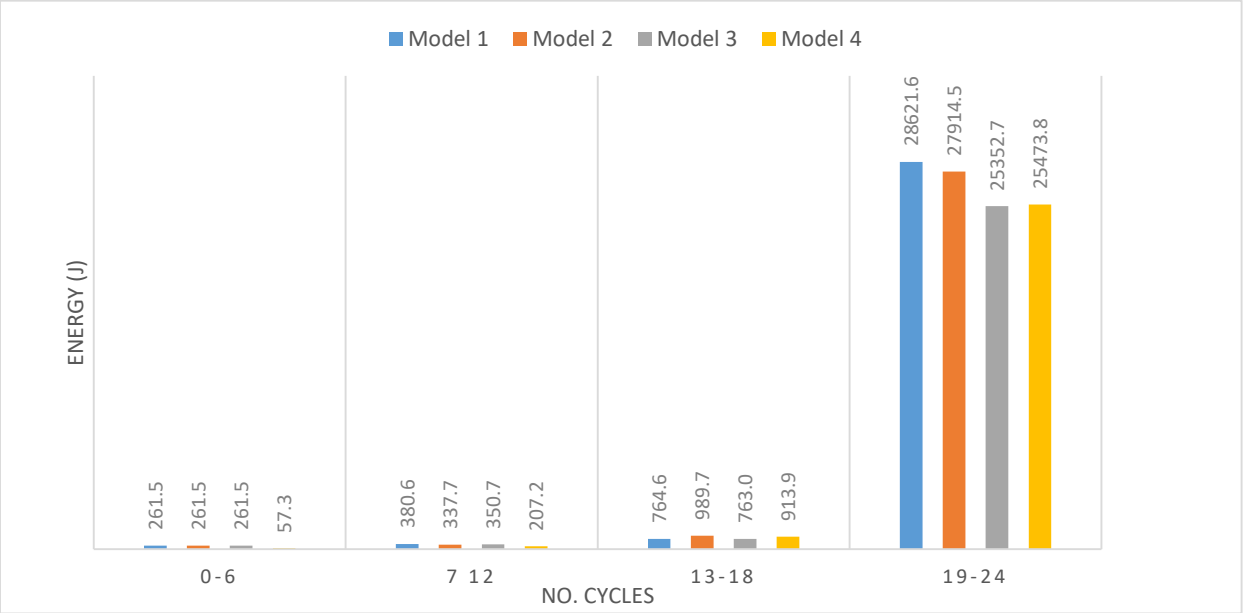

Figure 5.23: Energy dissipation by entire joint models.

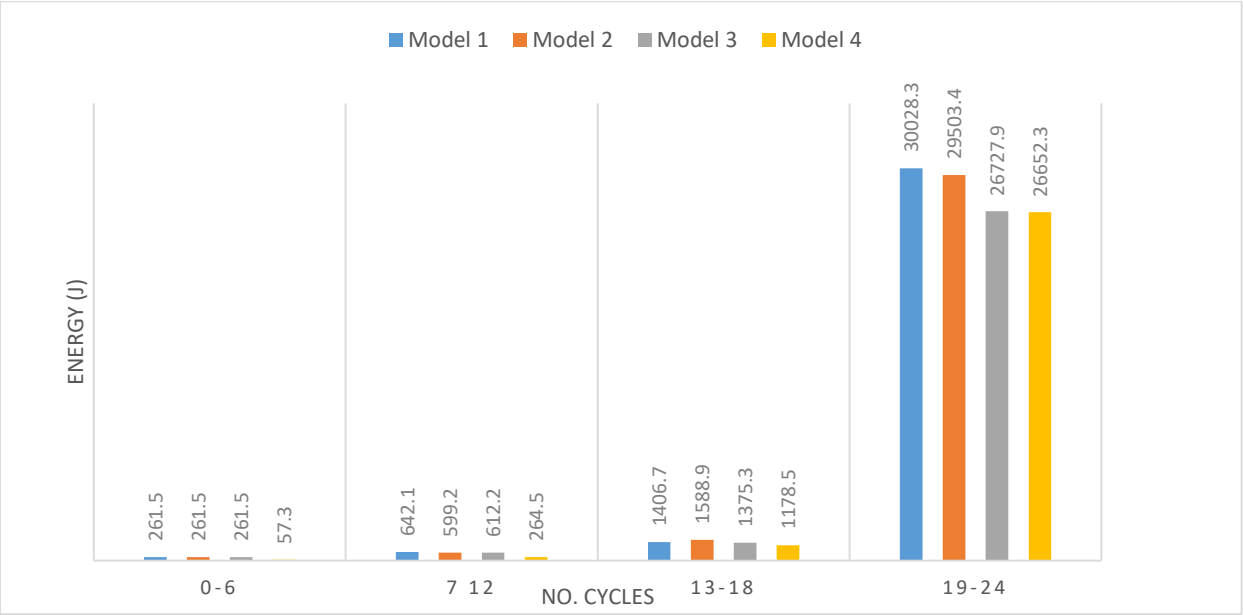

Figure 5.24: Accumulative energy dissipation by entire joint models.

Comparison between dissipated energy in column flange and dissipated energy in complete joint gives the awareness that column flange in bending plays an important role to dissipate the energy of whole joint. 30–45 % energy is dissipated by column flange in bending component of joint model and the remainder energy is dissipated by other components.

6. Conclusions and Recommendations for Future works

6.1. Conclusions

In this thesis, a FEM analysis was undertaken to assess the monotonic and cyclic behaviour of the component stiffened column flange in bending in steel beam-to-column joints. A parametric analysis was accomplished where a β parameter corresponding to the ratio of the strength of mode 1 and mode 2 of the equivalent T-Stub model suggested by EN1993-1-8 was changed in the range [0.75, 1.25].

The analysis encountered convergence issues that prevented the collapse load being reached in the monotonic and in the cyclic analysis.

The comparison of the collapse load of the stiffness column flange in bending according to the equivalent T-Stub model and the behaviour of the FEM models that the collapse loads of the equivalent T-Stub model are 25-35% higher than the elastic limits of the FEM models.

The FEM models of the stiffened column flange in bending showed that, along the first 24 cycles of the loading protocol developed in the EQUALJOINTS project no strength degradation, no stiffness degradation and no pinching effects are to be expected from this component.

The parametric analysis showed that the β parameter has a small influence in the behaviour of the stiffened column flange in bending. It was found that higher β parameters may lead to larger energy dissipation capacity but the trend is not clear.

Finally, the comparison of the energy dissipation in the column flange in bending and in the overall model showed that the column flange in bending contributes to 30-45% dissipation of energy of entire tension region of the joint.

6.2. Recommendations for Future works

The bounds imposed by time requirements prevented a deeper analysis of the subjects accounted for in this thesis. For future works, it is believed that the following issues should be addressed:

- Use material models that take into account a combination of kinematic and isotropic flow rules to simulate the cyclic behavior of the steel more accurately;
- Perform experimental tests to calibrate the numerical models;
- Solve the convergence issues encountered that prevented from reach the collapse of the models;
- Assess the combined effect of the formation of modes 1 and 2 in end plate and column flange;
- Assess the performance of the column flange in bending using a complete beam-column joint model to evaluate the effect of the redistribution of internal forces in the impact of the response of this component and to assess its actual demand;

7. References

[1] CEN. Euro code 3: design of steel structures — part 1-1: general rules and rules for buildings. CEN, Brussels: European Committee for Standardization; 2005.

[2] CEN. Euro code 3: design of steel structures — part 1–8: design of joints. CEN, Brussels: European Committee for Standardization; 2005.

[3] A. Tsitos, A. Elghazouli, M. D'Aniello, S. Costanzo, R Landolfo, A. Stratan, G. Sabău, Dan Dubina, F. Gentili, C. Rebelo and L. S.s da Silva. Selection of loading protocols Deliverable d-p3-1. Rev. 01. February 2016

[4] L. Massimo, Rizzano G, S. Aldina, Simões da Silva L, Experimental analysis and mechanical modelling of T-stubs with four bolts per row. Journal of Construction Steel Research 101 (2014) 158-174.

[5] Faella C, Montuori R, Piluso V, Rizzano G. Failure mode control: economy of semi rigid frames. Proceedings of the XI European Conference on Earthquake Engineering. Paris; 1998.

[6] Faella C, Piluso V, Rizzano G. Cyclic behavior of bolted joint components Journal of Construction Steel Research 1998;46(1-3) [p. paper number 129].

[7] Ciro Faella, Vincenzo Piluso, Gianvittorio Rizzano. Structural Steel Semi Rigid Connections: Theory, Design, and Software, WF. CHEN, CRC Press

[8] Piluso V, Rizzano G. Experimental analysis and modelling of bolted T-stub under cyclic loads. Journal of Construction Steel Research 64 (2008) 655-669.

[9] Swanson JA, Leon RT. Bolted steel connections: tests on T-stub components. Journal of Structural Engineering, ASCE 2000;126(1):50–6.

[10] Jaspart J-P, Weynand K. Design of joints in steel and composite structures, published by ECCS – European convention constructional steelwork; 2016.

[11] Hugo Renato Gonçalves da Silva Augusto. Characterization of the behaviour of partial-strength joints under cyclic and seismic loading conditions. PhD thesis, Coimbra, Portugal, 2017.

[12] Zeotemeijer P. A design method for the tension side of statically loaded, bolted beam-to-column connections. Heron Vol. 20 1974 no.1.

[13] J.P. Jaspart, J.F. Demonceau. Structural joints with more complex geometry and loading. Steel Connection Design – SUSCOS 1C2 Course – September 2016

[14] Dieter Declerck. Comparison between the Euro code methodology and a finite element model: the equivalent T-Stub method. MSc thesis, Gent, Belgium, 2016-2017

[15] Muhammad Asghar Bhatti. Fundamental finite element analysis and applications. John Wiley & Sons Inc. 2005.

[16] Simulia, "Getting Started with ABAQUS: Interactive Edition," Get. Started with ABAQUS Interact. Ed., p. 4.50-4.54, 2012.

[17] "Recommended testing procedure for assessing the behaviour of structural steel elements under cyclic loads", ECCS-Technical Committee 1 - Structural safety and loadings technical working group 1.3 - Seismic design. First edition.